Quantifying suspended sediment using multi-frequency echosounder measurements

Assessing the potential of single instrument sediment concentration inversions that account for variations in particle size

R.A.J. Jaarsma

TU Delft

NORTEK

Quantifying suspended sediment using multi-frequency echosounder measurements

Assessing the potential of single instrument sediment concentration inversions that account for variations in particle size

By

R.A.J. Jaarsma

in partial fulfilment of the requirements for the degree of

Master of Science
in Civil Engineering

at the Delft University of Technology,
to be defended publicly on January 24th at 11:00 AM.

Student number:	4470559	
Project duration:	February 2022 – January 2023	
Thesis committee:	Dr. Ir. M.A. de Schipper	TU Delft, Chair
	MSc. M. Daugharty	Nortek, supervisor
	Ir. M.A. van der Lugt	TU Delft, supervisor
	Dr. Ir. B.C. van Prooijen	TU Delft

An electronic version of this thesis is available at http://repository.tudelft.nl/.

TU Delft

NORTEK

Preface

Ever since spending holidays at the beach in Zeeland in my youth, I am fascinated by the Dutch coastal system and our history of providing flood safety. The decision to study Hydraulic Engineering in Delft followed naturally, and already during my BSc programme, I got fascinated by measurements and fieldwork. I recommend every student to pursue fieldwork as part of their programme at least once. For example, learning about a 1 m high significant wave height in class is one thing, but it is no substitute for first-hand experience in the field.

It was during flow measurements using a small boat, as part of the fieldwork course and internship at Nortek in September 2021, that my interest in capturing suspended sediments was caught. In discussions with my supervisors and colleagues at Nortek I learned about the possibilities and limitations of deriving sediment concentrations from vessel-based echosounder measurements. Researching the possibilities to enhance this technique using multi-frequency measurements as my graduation topic has been a great decision. Upon completing this report, I look back with a great feeling of fulfilment to have contributed to the development of this technique. The project involved taking echosounder and water sample measurements around the coastal waters of Texel, spending days in the lab analysing the samples, and processing the data and writing the report at the Nortek office in Hoofddorp.

I want to thank my company supervisor Maeve Daugharty for her enthusiastic support during the project and helping me develop skills like scientific writing and time management. Also, thank you Marlies van der Lugt, my university supervisor, for frequently dedicating time for brainstorm sessions in Delft and during the fieldwork activities at Texel. Being able to ask for guidance and feedback often truly helped completing the project with success.

I also want to thank Chair of the committee Matthieu de Schipper, committee member Bram van Prooijen and advisor Sicco Kamminga for their contribution in the project during the committee meetings and discussions at the university and office. Using their expertise, they helped me focus and think critically, resulting in a report of the desired level. I also want to thank Sicco for the internship and thesis opportunities at Nortek, as well as introducing the subject of multi-frequency echosounder measurements.

Regarding the fieldwork, data analysis and writing process, it would not have been possible if I did not receive all the help from everyone involved. Thank you Marlies, Maeve, colleagues Herman Huitema and Maarten Mulder, Meike Traas, Jaap van Duin and my good friend Maris Philippa for making the fieldwork a success. Also, I want to express my gratitude to NIOZ for offering the possibility of using their harbour and providing assistance during the time at Texel, and to my colleagues of Nortek for the great discussions, feedback and laughs at the office.

I am grateful for the support of my parents throughout my studies, starting when I just moved to Delft at age 17 not knowing what would come next, up to finding my path in the first steps of my professional career. Finally, thank you Flip de Granada for taking me on flights along the North Sea coast and Wadden Sea, allowing for unique impressions and a great cover photo.

R.A.J. Jaarsma
Delft, January 2023

Abstract

Direct measurements of suspended sediment concentration (SSC) are key in understanding sediment processes, for example to calibrate and validate numerical models in coastal morphology studies and to mitigate impact of dredge plumes. Traditional measurement methods such as in-situ water sampling and using optical backscatter sensors are labour intensive and flow intruding, which limits temporal and spatial resolutions that can be captured. Acoustic Doppler current profilers (ADCPs) are used to overcome these limitations by linking backscatter measurements to SSC. In addition, simultaneous flow measurements enable the possibility to capture sediment fluxes in a single instrument.

Current single frequency backscatter measurements require frequent reference measurements due to the dependency on particle size and other sediment characteristics. This limits the potential of ADCP sediment characterization in situations with substantial variations in sediment class, such as estuaries and around dredging operations. A method to account for particle size variations is the use of multi-frequency measurements: particle size estimates can be derived based on the acoustic wavenumber-particle size relation. Potential of this technique was previously obstructed due to spatial and temporal discrepancies induced by slanted beam backscatter measurements taken with separate instruments. Adding a vertical beam echosounder capable of high-resolution, multi-frequency measurements to the Nortek Signature 1000 ADCP enables co-located measurements in a single instrument.

To explore the potential of multi-frequency echo sounding for sediment concentration measurements, the instrument was tested in the coastal waters around the Dutch barrier island Texel. Backscatter measurements were obtained at 1000, 500 and 250 kHz, along with water sample reference measurements. The 1000 and 500 kHz measurements were used to compare performance of single and multi-frequency SSC inversions. The 250 kHz measurements were disregarded due to low signal-to-noise ratios.

Sound single frequency 500 kHz SSC inversions ($r^2 = 0.88$) were obtained only under steady measurement conditions where changes in sediment size class were assumed to be limited. When SSC was inferred over varying measurement conditions, assumed to contain sediment of ranging size classes, poor correlation with reference measurements ($r^2 = 0.33$) was obtained. Due to acoustic wavelength-particle size interactions, lower correlations were obtained for single frequency SSC inversions based on the 1000 kHz measurements.

Particle size estimates were obtained by combining the 1000 and 500 kHz measurements. Limitations were observed in the resolvable range of particle sizes due to a region of ambiguous solutions, introduced by the limited interval between the frequencies. In addition, uncertainty was introduced by using an uncalibrated echosounder and not verifying with true particle sizes. Application of the particle size estimates in the multi-frequency SSC inversion to compensate for changes in sediment size class did substantially improve correlations under varying measurement conditions ($r^2 = 0.89$). Hence, single instrument, multi-frequency echosounder measurements show potential to significantly increase performance of ADCP SSC inversions in conditions where variations in sediment size class occur.

Further validation is required to utilize the full capacity of measuring sediment fluxes using multi-frequency echosounder equipped ADCPs. This involves increasing certainty in particle size estimates by applying a larger frequency interval, using a calibrated echosounder and verifying particle size estimates with true values. In addition, performance of SSC estimates under conditions with ranging sediment class should be further statistically validated.

Index

Nomenclature

Term	Description
SSC	Suspended sediment concentration [mg L^{-1}]
ADCP	Acoustic Doppler current profiler
OBS	Optical backscatter
ABS	Acoustic backscatter
LISST	Laser in-situ scattering and transmissometer
SF	Single frequency
MF	Multi-frequency
Rx	Uncorrected backscatter [dB]
TS	Target strength [dB re 1 m^2]
S_v	Absolute volume backscatter [dB re 1 m^{-1}]
$S_v{}'$	Relative volume backscatter [dB]
PL	Power level [dB]
TL	Transmission loss [dB]
NT	Noise threshold [dB]
G	Calibration gain [dB]
R	Measurement range [m]
α_w	Signal absorption in water [dB/m]
α_s	Signal attenuation due to suspended sediment [dB/m]
k	Acoustic wave number [m^{-1}]
F	Acoustic frequency [Hz]
λ	Acoustic wavelength [m]
τ	Signal pulse length [m]
c	Sound speed through water [m/s]
r	Transducer radius [m]
M_s	Suspended sediment concentration [kg/m^3]
a_s	Particle radius [m]
ρ_s	Particle density [kg/m^3]
n_b	Number of scattering particles per unit volume [m^{-1}]
σ_{bs}	Backscattering cross-section [m^2]
f	Form function
K_1	Accounts for particle size-acoustic wavelength interaction
K_2	Accounts for particle shape and density
A	Backscatter model fitting parameter (SF and MF method)
B_{SF}	Backscatter model fitting parameter (SF method)
B_{MF}	Backscatter model fitting parameter (MF method)
β	Backscatter model fitting parameter (MF method)
r^2	Correlation coefficient
$RMSE$	Root mean square error

1 Introduction

1.1 Relevance of capturing suspended sediment transport processes

Understanding sediment transport processes is key in environmental management of estuaries and coasts. From large scale processes that drive estuarine budgets to small scale sediment fluctuations that occur during dredging operations, quantifying sediment dynamics plays a crucial role. Numerical models are a widely used tool in capturing these processes, however, in-situ monitoring is often required for model setup, calibration, and validation. Methods and technology that limit the need for these labour-intensive activities are becoming increasingly important.

1.1.1 Coastal management

Coastal zones are key in providing flood protection and offer great value to ecology and recreation. Extensive maintenance programmes exist to mitigate effects of sea level rise and changes due to human interventions. For example at the North Sea coast of the Dutch barrier island Texel (lower part of Figure 1), nourishments are carried out frequently to counteract erosion due to the strong tidal currents in the Molengat channel (Cleveringa, 2001). A recent development is the retrofitting of nourishments to flood sensitive coasts with sediment different to endemic material. An example is the Prins Hendrikzanddijk (PHZD) (middle part of Figure 1) at the Southern coast of Texel, placed in 2019 to replace the old disapproved sea dike (Fordeyn et al., 2020).

Understanding the effect of such human interventions on the morphologic development of the estuaries including the Wadden Sea (upper part of Figure 1) requires thorough investigations into sediment transport processes. Characterization and quantification of sediment budgets – how much sediment is imported or exported through inlets – is a key component. Due to the complexity of these systems, direct measurements are required for numerical model validation and calibration (Wang et al., 2012). However, these measurements are scarce and generally do not distinguish particle size fractions. At a minimum, distinguishing between mud ($d < 63$ µm) and sand ($63 < d < 2000$ µm) would give rise to better understanding of the morphodynamic processes (Pearson et al., 2021; Wang et al., 2012).

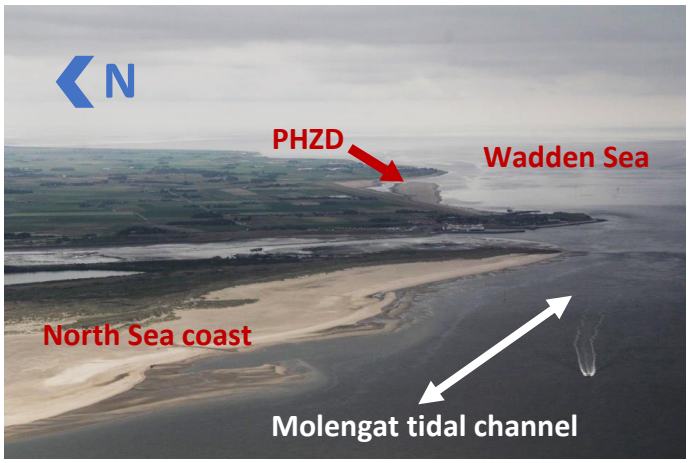

Figure 1: Aerial photo of the Dutch barrier island Texel that resides on the interface of the North Sea to the West and the Wadden Sea to the South. The retrofit Prins Hendrikzanddijk coastal protection is indicated in the middle.

1.1.2 Turbidity monitoring during dredging activities

High turbidity levels introduced by dredging activities can be devastating to surrounding areas. To reduce impact, numerical models are used for plume simulation. Due to the complex composition of sediment size classes in plumes (Figure 2) – e.g. coarse bed aggregates that are stirred up and fine floc forming sediment that settles in the water column (Smith & Friedrichs, 2011) – small-scale variations in particle settling velocities are present and require thorough investigation to reduce uncertainty in numerical models.

Therefore, efforts have been put into improving direct monitoring methods to capture the complex sediment transport processes, with the purpose of improving the ability to predict and reduce the impact of turbidity plumes on sensitive habitats (Smith & Friedrichs, 2011).

Figure 2: Turbidity plume introduced by dredging activities in the Waddenzee.

1.2 Measuring suspended sediment concentrations

1.2.1 In-situ water samples and optical backscatter measurements

A traditional method to determine SSC is to take in-situ water samples using bottles or by pumping and to analyse for SSC. The main drawback of using water samples is the poor temporal and spatial resolution that can be achieved due to the method being very labour intensive (Wren et al., 2000). Also, the local flow is disrupted during sampling which potentially leads to biased measurements.

For continuous measuring, optical backscatter (OBS) sensors are used: by defining a relation between optical backscatter intensities and known SSC values through lab measurements or field samples, the OBS signal is linked to SSC. OBS is most sensitive to fine mud particles (Pearson et al., 2021) and less responsive to coarser particles like sand. A laser in-situ scattering and transmissometer (LISST) is based on the same principles but uses laser instead of light and can be used not only to estimate SSC but particle size as well. LISSTs are effective with fine sediments and impose increasing errors for larger particles (Gartner et al., 2001). Like the water sampling

method, optical and laser measurements are flow-intrusive because of limited measuring range. Another drawback is that they are vulnerable to biofouling (Wren et al., 2000).

1.2.2 Acoustic backscatter measurements

Acoustic instruments are applied to overcome limitations of in-situ samples and OBSs. SSC profiles can be obtained over depth using measured backscatter intensities in stationary or vessel-mounted setups – depending on the need to measure at high temporal and/or spatial resolutions.

Instruments that have been used for this purpose include acoustic Doppler current profilers (ADCPs) (Deines, 1999; Gartner, 2004; Hoitink & Hoekstra, 2005; Kim & Voulgaris, 2003; Merckelbach & Ridderinkhof, 2005; Reichel & Nachtnebel, 1994), multi-beam echosounders (MBES) (Fromant et al., 2022; Simmons et al., 2010) and multi-frequency acoustic backscatter (ABS) systems, designed for capturing near-bed sediment processes (Thorne & Hardcastle, 1997; Vincent et al., 1999). The underlying principle in these applications is similar: a transducer emits an acoustic pulse (a ping) along a beam into the water. Depending on the presence of suspended sediment, organic matter, fish, bubbles and other material within the beam, part of the ping is backscattered to the transducer. SSC estimates are then obtained by linking backscatter intensity to the specific sediment properties via a model, for which – like optical instruments – reference measurements are often required (Reichel & Nachtnebel, 1994).

In case of the ADCP, backscatter is recorded as a by-product of the signal that is required for flow velocity measurements and is obtained in bins over depth. This makes the ADCP a promising instrument for monitoring sediment fluxes as SSC and flow velocity can be captured using the same instrument (Gray & Gartner, 2009). An example of this potential was demonstrated in Cutroneo et al. (2014), where stationary ADCP measurements were used to continuously monitor the effect of dredging activities in a harbour close to a sensitive area. In case turbidity levels exceeded a certain threshold combined with critical flow velocities into that direction, a warning was sent automatically to held dredging activities.

1.2.3 Limitations of single frequency echosounder measurements

The model that relates acoustic backscatter to SSC takes into account sediment characteristics, including the size of the backscattering particles (Crawford & Hay, 1993). With single frequency acoustic backscatter instruments, variations in sediment sizes cannot be resolved and reference measurements need to be acquired frequently if significant variations are present. This limits the potential of using acoustic instruments to characterize suspended sediment processes in coastal research and dredge plume monitoring applications like those mentioned in Section 1.1.

Therefore, multi-frequency ABS systems have been developed and based on the principle that different frequencies respond differently to particle size variations, the mean size and concentration of the particles can be derived from the multi-frequency signal (Crawford & Hay, 1993; Hay & Sheng, 1992; Thorne et al., 1991; Thorne & Hanes, 2002; Thorne & Hardcastle, 1997). Currently available multi-frequency ABS systems are designed to capture near-bed sediment transport processes and due to the use of high acoustic frequencies, have a relatively short measurement range of < 1 to 10 meters (Aquatec, 2018).

1.2.4 Multi-frequency ADCP measurements

To capture sediment transport processes over a larger part of the water column and to derive transport fluxes based on simultaneous flow velocity measurements, research has been carried out in applying the multi-frequency method on coupled ADCPs measuring at different frequencies. In Guerrero et al. (2012) two ADCPs, one measuring at 1200 kHz and another at 600 kHz, were deployed in a controlled lab environment yielding estimations of grain size and concentration that showed good agreement with true values. The method was then applied in a river study, where the results suggested good agreement with sample-derived reference data (Guerrero et al., 2013). Coupled with flow velocity measurements, the re-suspension of bed load and the transport of fine suspended sediment higher in the water column were captured, illustrating the potential of the technique.

More literature on river applications is available, some of which containing methods to account for acoustic attenuation in environments of high SSC (Moore et al., 2013; Topping et al., 2007; Topping & Wright, 2016). Coastal deployments have been carried out as well, for example Jourdin et al. (2014), where a set of ADCPs was deployed close to the French Atlantic coast. Although the multi-frequency derived SSC estimates did not show improved results in comparison to the traditional single frequency method, small mineral particles were successfully distinguished from larger organic particles based on particle size. The methodology was later repeated in a deployment in the coastal waters of Senegal (Floc'H et al., 2019).

1.2.5 Limitations of current multi-frequency ADCP measurements

While potential of the multi-frequency method was indicated, spatial and temporal variations between instruments constrain further development. In case of the deployment in the French Atlantic coast, the distance between the instruments was as high as 50 meters (Jourdin et al., 2014) in an environment where spatial variation of the suspended sediment processes typically is much denser. Guerrero et al. (2013) introduces concerns regarding differences in temporal and vertical resolution between the ADCPs.

Another concern is related to ADCPs being designed for 3D flow velocity measurements, for which pings are emitted and received along slanted beams, typically at a relatively coarse resolution of 0.25-0.5 m (Guerrero et al., 2013). This configuration is sub-optimal for capturing suspended sediment, for which a vertical beam orientation is preferred (Guerrero et al., 2013; Jourdin et al., 2014) with a denser resolution to capture small-scale vertical variations in SSC (Guerrero et al., 2012).

1.2.6 Single instrument, multi-frequency measurements

The Nortek Signature 1000 ADCP was adapted to capture suspended sediment via a vertically-orientated fifth beam capable of recording backscatter intensities in bins of 3 mm or larger (Nortek, 2022b). With this configuration, it is possible to resolve suspended sediment structures in more detail and to measure closer to the water surface or bed (van der Grinten, 2019). The next step in the development of using ADCPs to capture suspended sediment is to enable multi-frequency measurements on a single instrument, overcoming the practical limitations that are involved with using separate instruments. To this end, a Nortek Signature 1000 ADCP was adapted to measure at 1000, 500 and 250 kHz. Therefore, it has potential to obtain simultaneous measurements of particle size, SSC and flow velocities.

1.3 Thesis objective and scope

The goal of this thesis is to demonstrate the potential of a method using multi-frequency echosounder measurements taken with a single instrument and comparing performance with its single frequency measurements. Based on echosounder theory and previous work on the subject, the required steps in setting up instrumentation, obtaining reference measurements and the data processing procedure will be introduced, as well as the applicability and limitations of the method. Performance will be assessed based on field measurements comparing the single and multi-frequency methods. Assessing the validity of particle size estimates is not covered by the scope of this thesis and is left for further research. The same applies to the concept of accounting for signal attenuation in conditions of high SSC and coupling of flow velocity measurements.

1.4 Research questions

The research question is stated:

What is the added value of single-instrument, multi-frequency echosounder measurements in quantifying suspended sediment compared to single frequency measurements?

To answer this question, sub-questions include:

1. Under what conditions can SSC successfully be estimated using single frequency echosounder measurements and what are the limitations of the method?
2. How can mean particle size be derived from multi-frequency echosounder measurements?
3. To what extend does the multi-frequency method overcome the limitations of the single frequency method?

1.5 Research approach and thesis outline

The required concepts of inferring SSC from acoustic backscatter measurements are introduced in Chapter 2. For the single and multi-frequency method, involved parameters and methods to resolve them are discussed. Then, performance of both methods is assessed using field measurements taken in the coastal waters around Texel (Figure 1) with a vessel-mounted single-instrument setup. Details about data collection and processing are discussed in Section 3, while results are presented and discussed in sections 4 and 5 respectively. Finally, research findings are concluded in Chapter 6.

2 Theoretical background

In this chapter, the basics of inferring SSC from acoustic backscatter measurements are introduced. Starting with the sonar equation, the process of accounting for signal losses is covered, followed by the introduction of the general backscatter model that relates sediment properties to backscatter intensities. Finally, methods to solve for SSC based on this model using single and multi-frequency measurements are presented. An overview of these concepts is given in Section 2.5.

2.1 Echosounder principles

2.1.1 Sonar equation

Sources of backscatter are characterised in terms of target strength (TS, [dB re 1 m^2]) or volume-backscattering strength (S_v, [dB re 1 m^2 m^{-3}]), which are based on the backscattering cross-section (σ_{bs} [m^2]) and other characteristics of the backscattering source (Echoview, 2022). TS measures signal intensity for individual objects like fish (Echoview, 2022) while S_v is generally used to capture suspended sediment, linking signal intensity to a certain backscattering cross-section within a volume. Writing the active sonar equation (Urick, 1983) in terms of S_v yields a formula to correct received signal intensities (R_x) for losses (S_e) and environmental noise (NT) (Equation 1) (Nortek, 2022a):

$$S_v = 10\log_{10}\left(10^{\frac{R_x}{10}} - 10^{\frac{NT}{10}}\right) + S_e + G \quad (1)$$

G represents gain, an instrument calibration factor which is further discussed in Section 2.1.3. Defining NT is explained in Section 2.1.4 and signal losses are determined with Equation 2:

$$S_e = 20\log_{10}(R) + 2\alpha R - 10\log_{10}\left(\frac{c\tau}{2}\right) + PL - 10\log_{10}\left(\frac{5.78}{k^2 r^2}\right) \quad (2)$$

where

- $20\log_{10}(R)$ accounts for acoustic beam spreading at distance R from the transducer;
- $2\alpha R$ compensates for signal attenuation due to absorption by water and sediment, with α being the absorption coefficient [dB/m];
- $10\log_{10}\left(\frac{c\tau}{2}\right)$ is a term called *target reflectivity* and contains the speed of sound through water, c, and the signal pulse length, τ;
- $10\log_{10}\left(\frac{5.78}{k^2 r^2}\right)$, the equivalent beam angle, corrects for the effect that not every particle within the sampling volume contributes equally to R_x due to its displacement from the beam axis. This term contains the acoustic wave number, k, and transducer radius, r;
- PL is the echosounder power level.

2.1.2 Signal attenuation

The signal attenuation term in Equation 2 includes absorption by water (α_w) and suspended sediment (α_s):

$$\alpha = \alpha_w + \alpha_s \quad (3)$$

α_w is determined relatively straight-forward and depends on the acoustic frequency, salinity, temperature and pressure (Gartner, 2004; Schulkin & Marsh, 1962). Determining α_s is more

complicated because besides the acoustic frequency, it also depends on the size and concentration of the suspended particles. The latter calls for an implicit solution when using acoustics to estimate SSC (Nortek, 2020). Some studies propose methods to estimate α_s based on water samples (Sassi et al., 2012) or by using multiple acoustic frequencies, with the purpose to characterize the present suspended sediment class using this estimate (Topping et al., 2007). In other cases, attenuation by suspended sediment is assumed negligible in comparison to water attenuation, except for when concentrations are very high[1] (Gartner, 2004; Hay & Sheng, 1992).

2.1.3 Instrument calibration

In Equation 1, G accounts for variations in transducer performance and is instrument and frequency specific. In absence of G, measurements of *relative volume backscatter*, denoted as S_v', are obtained. With calibration measurements, absolute volume backscatter is obtained. In single frequency applications, SSC values can be derived by fitting S_v' to reference SSC measurements if the same instrument is used. If backscatter measurements are to be compared directly between instruments, absolute volume backscatter (denoted as S_v) measurements are required. Then, G can be determined by performing an instrument calibration in the lab[2] for each instrument and frequency, where applicable. Because the transducer can drift over time, G must be redetermined frequently (Demer et al., 2015).

2.1.4 Noise threshold

Another offset parameter is NT which contains instrument and background related noise levels:

$$NT = NT_{instrument} + NT_{background} \quad (4)$$

$NT_{instrument}$ is related to electrical noise of the instrument itself and is usually determined by the instrument manufacturer. $NT_{background}$ contains the level of noise caused by external factors during measuring. One way of estimating the latter is to take the measured R_x value in the last (couple of) cell(s) in each ping, corresponding to the deepest measured signal intensity where it is assumed that the transmitted pulse has been dissipated due to transmission losses[3]. Therefore, R_x will asymptotically tend to $NT_{background}$.

[1] For a 2400 kHz ADCP, α_s is in the same order of α_w only if $SSC \geq 1000$ mg/L for particles of 125 µm or larger (scattering losses), or 10 µm or smaller (viscous losses). For lower frequencies, the contribution of viscous and scattering losses are even lower (Gartner, 2004).

[2] A commonly applied instrument calibration procedure is the method using Tungsten spheres: a spherical element with predetermined σ_{bs} and TS is placed into the beam of the instrument at varying distances from the transducer (Demer et al., 2015; Nortek, 2022b).

[3] Only valid if the depth is large enough for the signal to be attenuated completely. In shallower waters, this might not be the case and NT should be determined differently.

2.2 Inversion of suspended sediment characteristics

Based on S_v measurements, SSC is derived using a model that describes the backscattering properties of suspended sediment considering specific particle properties. This includes particle concentration, size, shape and density.

2.2.1 General backscatter model

For spherical particles, volume backscatter is related to the mean backscattering cross-section $\langle \sigma_{bs} \rangle$ within a volume via:

$$S_v = 10 \log_{10}(n_b \langle \sigma_{bs} \rangle) \tag{5}$$

where n_b is the number of scattering particles per unit volume (Sassi et al., 2012). The concentration of the particles M_s is linked to the mean particle radius $\langle a_s \rangle$ via n_b:

$$M_s = \frac{4}{3} \pi \rho_s n_b \langle a_s^3 \rangle \tag{6}$$

Which can be rewritten as:

$$n_b = \frac{3}{4\pi \langle a_s^3 \rangle} M_s \tag{7}$$

$\langle \sigma_{bs} \rangle$ is related to $\langle a_s \rangle$ (Medwin & Clay, 1998):

$$\langle \sigma_{bs} \rangle = \frac{1}{4} \langle a_s^2 f^2 \rangle \tag{8}$$

Here, f is the so-called form function, and describes the backscattering behaviour based on the product of the acoustic wavenumber and particle radius $k a_s$ (Thorne & Meral, 2008) and is further discussed in Section 2.3.3. The terms written in $\langle \cdot \rangle$ denote mean values of backscattering particle characteristics within the ensonified volume. Rearranging equations 5 to 8 yields a relation between S_v and M_s (Sassi et al., 2012):

$$S_v = 10 \log_{10} \left(\frac{\langle a_s^2 f^2 \rangle}{\langle a_s^3 \rangle} \frac{3}{16 \pi \rho_s} M_s \right) \tag{9}$$

For spherical scatterers with homogeneous density ρ_s, M_s can be derived directly from S_v using Equation 9, provided that ρ_s, $\langle a_s \rangle$ and $\langle f \rangle$ are known, the instrument has been calibrated and suspended sediment-induced signal attenuation is negligible. In some cases, $\langle a_s \rangle$ is estimated based on the sediment present in the bed (Thorne & Hanes, 2002), supplementary measurements (Fromant et al., 2022) or previously obtained knowledge. However, in most cases information about the mean particle size and other sediment properties is not available and simplification of Equation 9 is required. It can be written in the form:

$$S_v = 10\log_{10}(K_1 K_2 M_s) \tag{10}$$

$$K_1 = \frac{\langle a_s^2 f^2 \rangle}{\langle a_s^3 \rangle} \tag{11}$$

$$K_2 = \frac{3}{16\pi\rho_s} \tag{12}$$

Here, K_1 accounts for the effect of particle size and the sediment backscattering behaviour through a_s and f, K_2 represents the shape and density of the particles.

2.3 Estimating SSC using single frequency measurements

2.3.1 Solving the reduced backscatter model

When S_v or S_v' measurements are taken at a single frequency and no auxiliary information about the sediment properties is available K_1 and K_2 cannot be resolved acoustically. To account for this, the model can be tuned to specific sediment properties within a measurement volume by solving for the unknown parameters using reference SSC measurements. First, the backscatter model is rewritten in the form:

$$S_v' = A \cdot 10\log_{10}(M_s) + B_{SF} \tag{13}$$

where $B_{SF} = 10\log_{10}(K_1 K_2) - G$ and A is introduced to describe the contribution of M_s to S_v'. In theory, $A = 1$ but in practise deviations are observed. Then, by calculating the right-hand side of Equation 13 for every reference measurement of M_s, A and B_{SF} can be determined by means of a linear regression. If there is little variation in sediment properties (size, shape, density), M_s can be estimated via:

$$M_s = 10^{\frac{S_v' - B_{SF}}{10A}} \tag{14}$$

When sediment properties vary too much, the SF approach yields poor performance in estimating SSC due to variations in K_1 and K_2 not being resolved for each measurement. Instead, average values are captured in B_{SF} based on the model fitted to the reference measurements.

2.3.2 Acoustic frequency – particle size interaction

Another factor that impacts performance of the SF method is the relation between the acoustic wavenumber (k) and the radius of the scattering particles (a_s). The acoustic wavenumber can be calculated through $k = \frac{2\pi F}{c}$, where F is the acoustic frequency and c is the speed of sound through water. The backscattering behaviour can be split into three regimes based on the wavenumber-particle size product ka_s (Echoview, 2022; Medwin & Clay, 1998).

For $ka_s \ll 1$, backscatter is in the *Rayleigh regime*. Then, the acoustic wavelength is much larger than a_s and the backscatter response is log-linearly related to ka_s. When $ka_s \approx 1$, the wavelength is on the order of a_s. Then, the sound waves start to interfere with each other which results in a complex pattern of backscatter peaks and troughs. This is referred to as the *interferential scattering regime*. Finally, the *geometric scattering regime* applies to $ka_s \gg 1$. Here, the wavelength is much smaller than a_s. The crucial difference with respect to the Rayleigh regime is that the sound waves are now reflected by the particle surface, instead of the volume

of the particle. The result is that the strength of the backscattered signal is not significantly dependent on a_s nor the acoustic frequency, and hence its product ka_s (Echoview, 2022).

For good performance of single frequency SSC estimations, measurements should be taken in the Rayleigh regime ($ka_s \ll 1$). At the same time, ka_s should be large enough to provide sufficient sensitivity to small (relative to the wavelength) particles (Lohrmann, 2001). This implies that for varying sediment size classes, different frequencies may be required for best results.

2.3.3 The form function of quartz sand

In a range of lab studies (Hay, 1991; He & Hay, 1993; Thorne & Buckingham, 2004; Thorne et al., 1995), the backscattering behaviour of quartz sand particles was analysed for ranging ka_s. Thorne and Meral (2008) combined the data (Figure 3) to which the form function (f) was fitted:

$$f(a_s) = \frac{(ka_s)^2\left(1 - 0.35e^{-\left(\frac{ka_s-1.5}{0.7}\right)^2}\right)\left(1 + 0.5e^{-\left(\frac{ka_s-1.8}{2.2}\right)^2}\right)}{1 + 0.9(ka_s)^2} \quad (15)$$

For values of $ka_s < 0.5$, $f \approx 1.25(ka_s)^2$, whereas $f \approx f_{\lim} = 1.1$ for $ka_s > 5$. For $0.5 \leq ka_s \leq 5$, f follows the bracketed terms in the numerator of Equation 15. Based on these measurements, the Rayleigh regime applies to $ka_s < 0.5$, $ka_s > 5$ captures the geometric scattering regime and the interferential regime is valid for values in between. For $F = 1000$; 500 and 250 kHz, the corresponding particle radii are given in Table 1. Note that these limits are based on the quartz sand form function, for other types of scatterers different values of ka_s may apply. In general, $ka_s \ll 1$ is used as the general Rayleigh regime upper limit.

F (kHz)	$a_{s,ka=0.5}$ *(μm)*	$a_{s,ka=1}$ *(μm)*	$a_{s,ka=5}$ *(μm)*
1000	120	240	1195
500	240	480	2385
250	475	955	4775

Table 1: Values of particle radius a_s for $ka_s = 0.5$, 1 and 5, indicating the different scattering regimes for varying frequencies based on lab measurements of the backscattering behaviour of quartz sand.

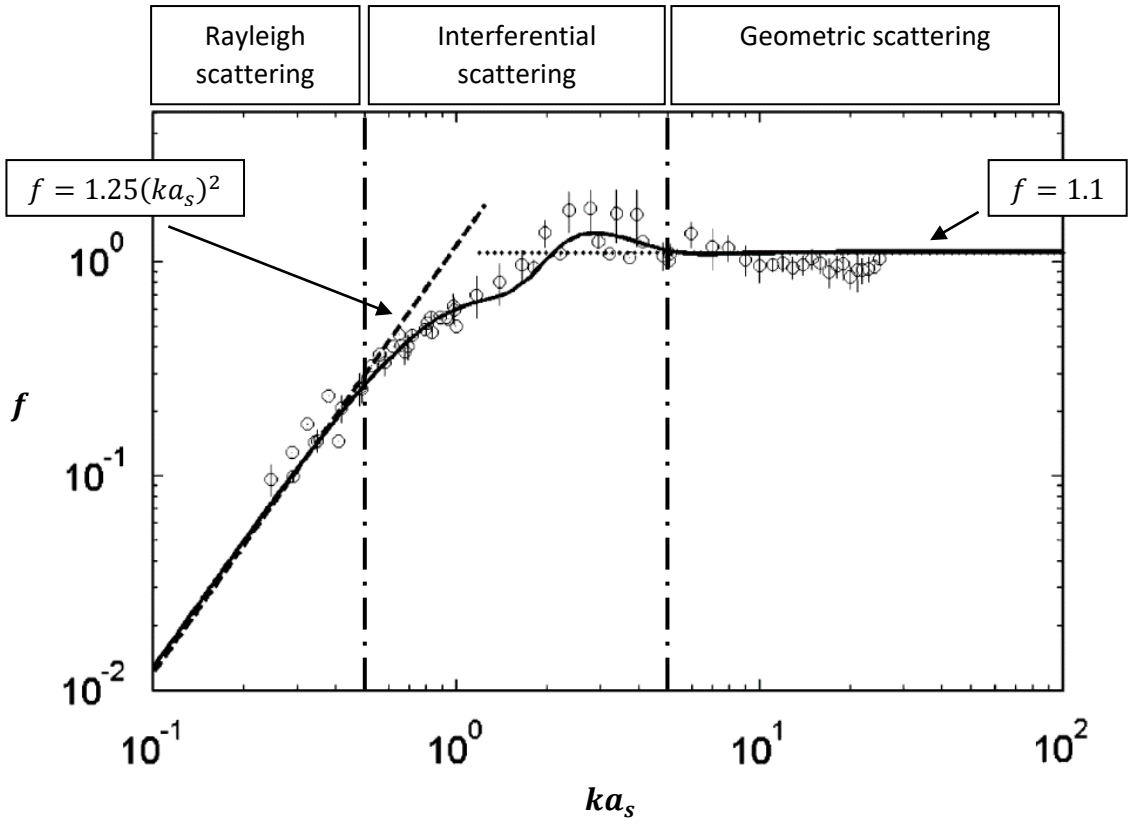

Figure 3: Backscattering behaviour of quartz sand for ranging values of ka_s. The dash-dotted lines delimit the Rayleigh, interferential and geometric scattering regimes. Based on lab experiments – indicated with circles – the backscattering form function (f; Equation 15) is defined and indicated by the solid line. For Rayleigh scattering, $f = 1.25(ka_s)^2$ (dashed line). In the geometric regime, $f = 1.1$ (dotted line). Figure taken and adapted from Thorne and Meral (2008).

2.4 Multi-frequency method

Multi-frequency backscatter measurements can be used to derive particle size estimates based on the wavenumber – particle radius relation described by the form function. This way, K_1 in Equation 10 can be resolved, allowing for SSC estimations that are less sensitive to variations in sediment characteristics.

2.4.1 Particle size derivation based on multi-frequency measurements

Based on the quartz sand form function, the varying response to a_s can be plotted for individual frequencies, e.g. 1000, 500 and 250 kHz (Figure 4). For constant a_s, different values of f correspond to different frequencies, with differences becoming smaller towards the boundaries of the Rayleigh scattering regimes (vertical dash-dotted lines in Figure 4). Hence, the form function ratio $\frac{f_{F_1}}{f_{F_2}}$ (with F indicating the acoustic frequency, and $F_1 > F_2$) can be linked to the particle radius a_s (Figure 5).

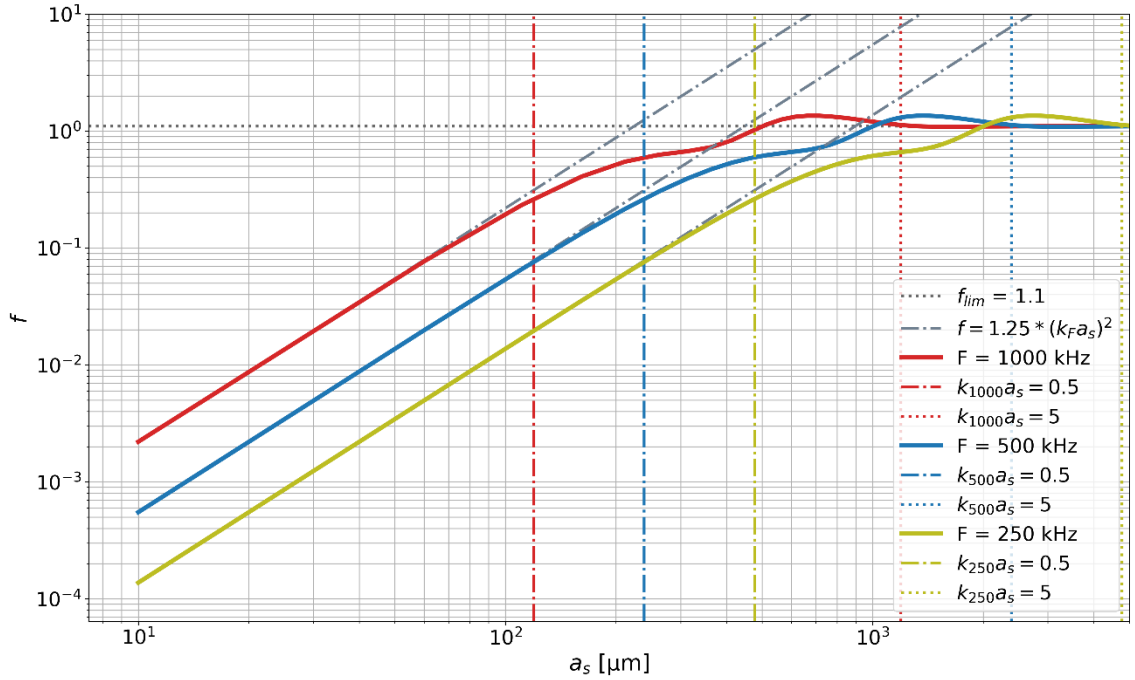

Figure 4: Form function for sand particles (Equation 15) plotted against a_s for F = 1000, 500 and 250 kHz and accompanying values of a_s corresponding to $ka_s = 0.5$ and $ka_s = 5$ to indicate the different scattering regimes. f-curves of lower frequencies are shifted to the right compared to higher frequencies, leading to higher boundaries of the scattering regimes.

The form function ratio is directly linked to measured volume backscatter differences between F_1 and F_2, denoted as ΔS_v. Writing the backscatter model (Equation 10) twice and subtracting gives:

$$S_{v,F_1} = 10\log_{10}\left(K_{1,F_1}K_2M_s\right) \tag{16}$$

$$S_{v,F_2} = 10\log_{10}\left(K_{1,F_2}K_2M_s\right) \tag{17}$$

$$\Delta S_v = 10\log_{10}\left(\frac{K_{1,F_1}}{K_{1,F_2}}\right) \tag{18}$$

In case of a unimodal and narrow particle size distribution (PSD) and homogeneous type of sediment, K_1 reduces to (Jourdin et al., 2014):

$$K_1 = \frac{f^2}{\langle a_s \rangle} \tag{19}$$

Then, the following relation with ΔS_v exists:

$$\Delta S_v = 10\log_{10}\left(\frac{f_1^2}{\langle a_s \rangle} / \frac{f_2^2}{\langle a_s \rangle}\right) = 20\log_{10}\left(\frac{f_1}{f_2}\right) \tag{20}$$

Under the assumption that the applied form function is representative of the sediment's backscattering behaviour and that particle sizes follow a narrow distribution, mean particle radius estimates can be derived from backscatter measured at two frequencies (Equation 20). For brevity, estimations of mean particle radii are denoted as a_s – without the brackets – in the remainder of this report. K_1 (Equation 11) can be determined for either of the frequencies used, where f is determined using a_s (Equation 15).

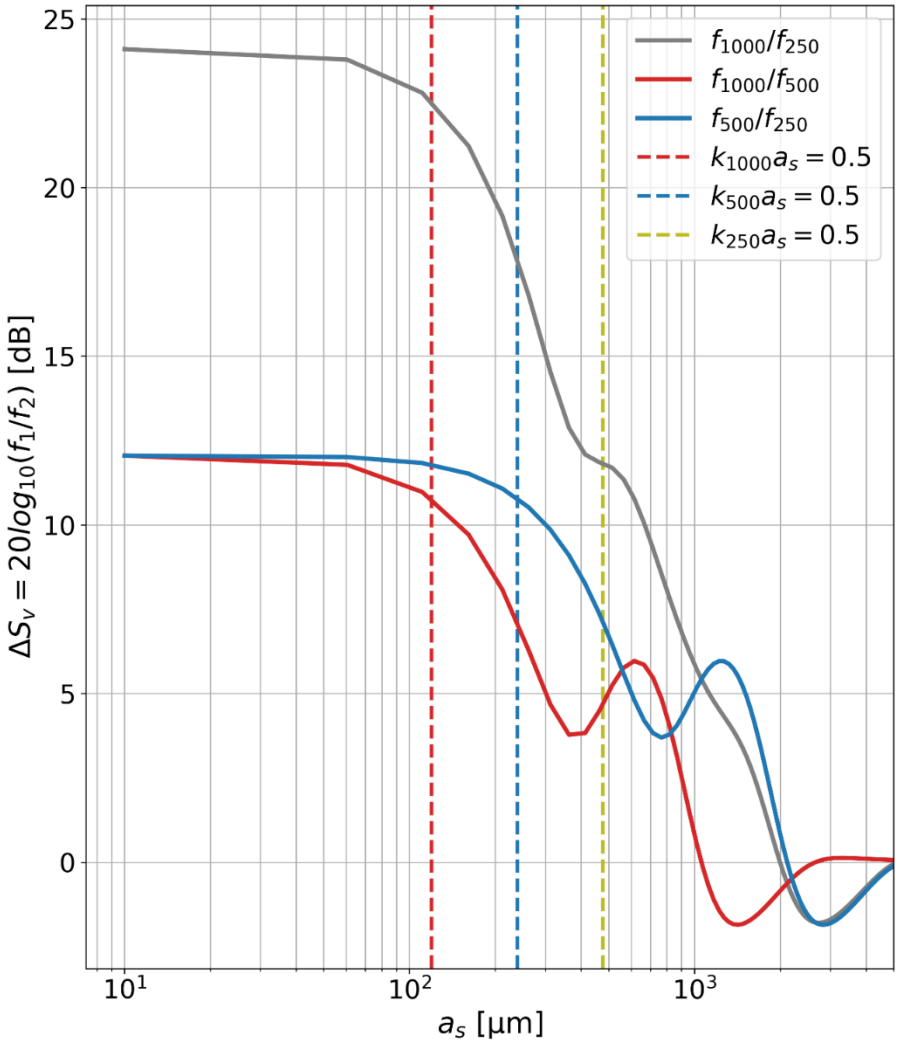

Figure 5: The form function ratio ($\frac{f_1}{f_2}$), determined from multi-frequency backscatter measurements, is related to the mean particle radius a_s. The range of a_s that can be resolved is bounded by the choice of acoustic frequencies, where a larger frequency interval increases the $\frac{f_1}{f_2}$ range, giving rise to more accurate estimations of a_s.

2.4.2 Resolvable range

The range of a_s that can be resolved via the form function ratio depends on the selection of F_1 and F_2: if the frequency interval remains constant, using a lower set of frequencies shifts the range upward, while the range is shifted in the opposite direction for a higher set of frequencies. A larger interval between the two acoustic frequencies potentially leads to more precise a_s estimations, because the $\Delta S_v - a_s$ relation is less sensitive: a small change in a_s is captured in a larger value of ΔS_v.

For the $\frac{f_{1000}}{f_{500}}$ and $\frac{f_{500}}{f_{250}}$ form function ratios, multiple solutions to a_s exist for the range of $3.7 < \Delta S_v < 6.0$ and $-1.9 < \Delta S_v < 0$ (Figure 5). Choosing a larger frequency interval reduces or overcomes this ambiguity. For example, the $\frac{f_{1000}}{f_{250}}$ ratio has an unambiguous solution range of $19 < a_s < 1980$ mm for $0.12 < \Delta S_v < 24$ dB.

When backscatter intensities are measured at more than two frequencies, multiple form function ratios are available. In case of an ambiguous solution to a_s, estimates based on the other ratios can be used for validation (Thorne & Hardcastle, 1997).

2.4.3 Multi-frequency SSC inversion model

With K_1 resolved, M_s can be derived directly from multi-frequency measurements assuming the particles are spherical and have a known uniform density ρ_s via:

$$M_s = \frac{16\pi\rho_s}{3}\frac{a_s}{f^2}10^{\frac{S_v}{10}} \tag{21}$$

In practice, variations in particle shape and density – captured in K_2 (Equation 10) – occur, which are not resolved with the MF method. Besides, the accuracy of the derived values of a_s may be limited due to the applied form function not sufficiently representative of the actual suspended sediment, and the assumption of a narrow PSD can be invalid.

To account for the potential limited applicability of the backscatter model in general form (Equation 10), fitting parameters are introduced:

$$S_v' = A \cdot 10\log(M_s) + 10\log_{10}\left(\frac{f^\beta}{a_s}\right) + B_{MF} \tag{22}$$

Where A is the same as in the SF method (Equation 13) and $B_{MF} = 10\log_{10}(K_2) - G$. In principle, calibrated echosounder measurements should be used to derive a_s from ΔS_v. Then, $S_v' = S_v$ and $B_{MF} = 10\log_{10}(K_2)$. β is introduced to account for the potentially limited accuracy of the a_s estimations (for the theoretical general model, $\beta = 2$). A, B_{MF} and β can be determined by means of a linear regression with reference SSC measurements. Then, M_s follows from:

$$M_s = 10^{\frac{\left(S_v' - 10\log_{10}\left(\frac{f^\beta}{a_s}\right) - B_{MF}\right)}{10A}} \tag{23}$$

2.5 Overview single and multi-frequency methods

The steps and assumptions involved with the SF and MF method to derive SSC from echosounder measurements can be summarized in a schematic (Figure 6). For the SF method, S_v' must be fitted to reference SSC measurements frequently. Then, transducer drift is accounted for and echosounder calibration is not required. However, if measurements between instruments are to be compared, calibration of both instruments should be carried out.

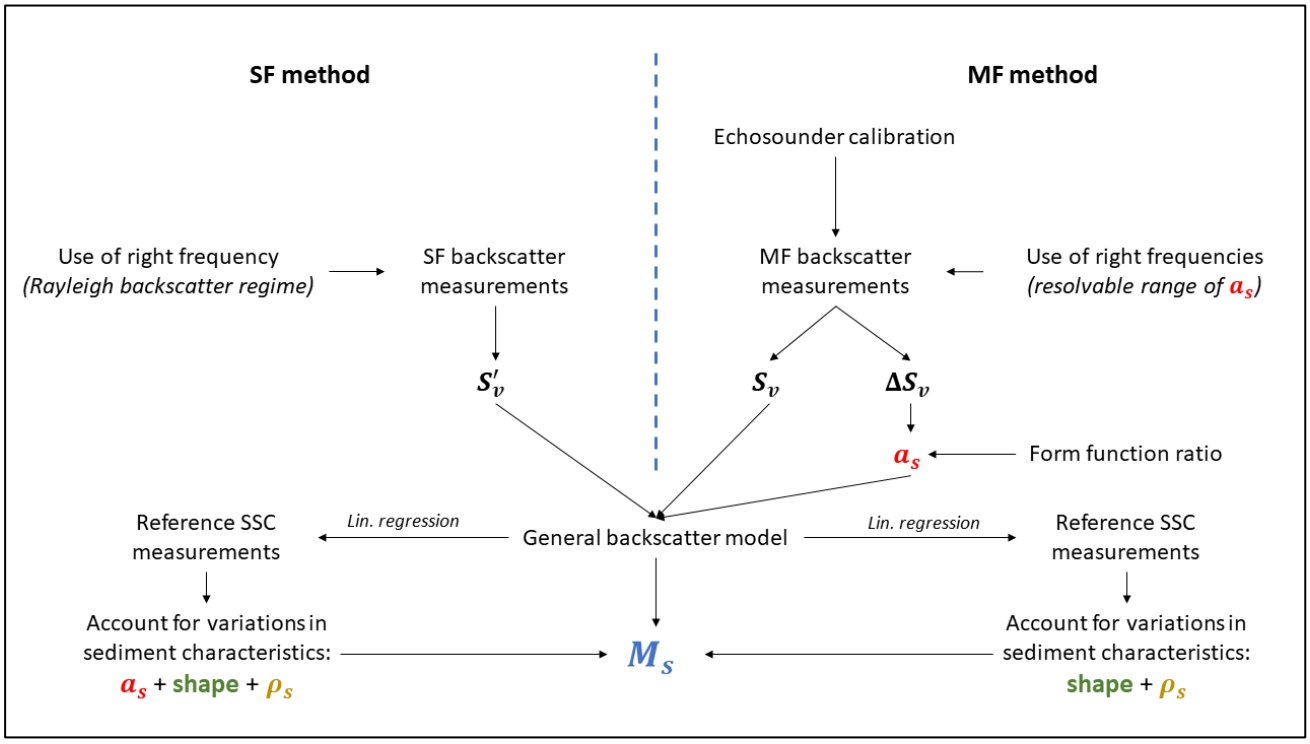

Figure 6: Overview of SF and MF method to solve the general backscatter model for M_s based on acoustic backscatter measurements.

3 Research method

3.1 Measurements

3.1.1 Field campaign

To determine the added value of single-instrument, multi-frequency echosounder measurements in comparison to single frequency measurements, both methods were applied during a field campaign in the coastal waters around Texel in May and June 2022. At several locations (Figure 7), backscatter profiles were taken using a vessel mounted ADCP in depths ranging from 5 to 20 m. In addition, reference measurements were obtained by taking water samples which were analysed in the lab for SSC.

Figure 7: Overview map of measurement locations, including Het Molengat (MG), Marsdiep (MD), Prins Hendrikzanddijk (PHZD) and Waddenzee (WZ). Map source: Google Maps.

3.1.2 Echosounder measurements

The instrument – a Nortek Signature 1000 ADCP as part of the Nortek VM 1000 Coastal package – was configured to alternately ping at 1000, 500 and 250 kHz at a 2 Hz sampling rate using its central transducer. Flow velocities were also captured but not further studied. For each echosounder frequency, the cell size was set to 0.05 m, the transmit pulse length 0.1 m and pulse compression was not applied. Backscatter was measured at a 0.01 dB resolution (Nortek, 2022c). While taking water samples, backscatter measurements were taken continuously and colocated in the data processing stage later (Section 3.2.2).

a) b)

Figure 8: a) Picture of the measurement boat 'De Waterwolf' with the Nortek Signature 1000 ADCP mounted to the port side, with the instrument raised out of the water for transporting. b) Picture of measurement setup, taken aboard the vessel. Here, the instrument is deployed. The GNSS antenna, visible in the top left, was used to log sampling locations and to correct measured flow velocities for vessel speed. The computer and monitor located in the cabin were used to monitor and store the data.

3.1.3 Reference measurements

Reference SSC measurements were obtained by taking water samples using a Niskin bottle (Figure 9a) and pumping system (Figure 9b). Sampling depths were recorded using a RBR Solo pressure sensor attached to the bottle and tube end connected to the pump. Using the Niskin bottle, water samples of around 2 to 2.5 litre were obtained at varying depths. The pumping system was used to obtain near-bed samples of around 3 L at a rate of 1.5 L/min.

Aboard, the samples were sieved to divide between fine and coarse particles using a mesh size of 63 or 75 µm. The coarse material retained on the sieve was flushed with fresh water and stored in a container. The sieved water volume was stirred, from which a 0.5 L subsample was taken and stored in a bottle. SSC values for the fine and coarse particles were determined following the lab procedure described in Appendix B and combined to obtain total SSC.

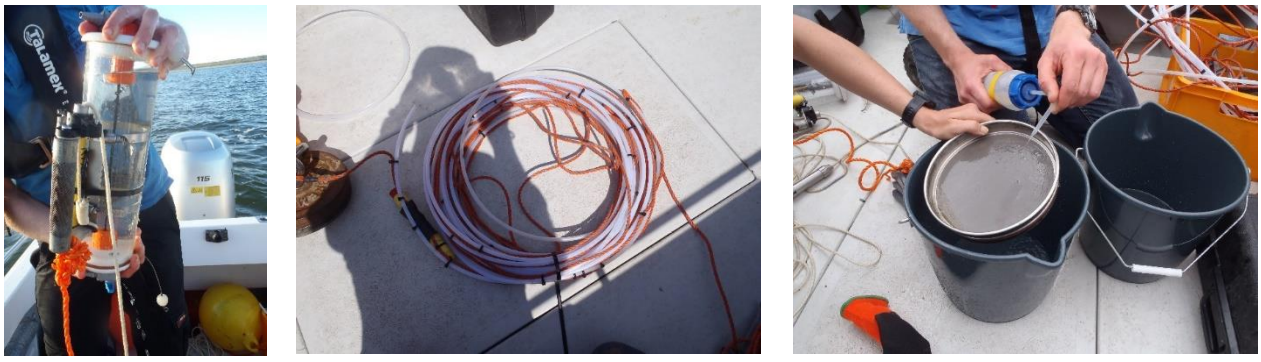

a) b) c)

Figure 9: a) Niskin bottle used for water sampling to determine SSC. The sampling depth was derived from pressure sensor data. b) Sampling tube with pressure sensor attached. c) Sieving to separate suspended particles based on particle size.

3.2 Data analysis

3.2.1 Measurement subsets

To limit variations in sediment characteristics and deviations in sampling methods, only the Niskin bottle water samples and accompanying backscatter measurements taken at *Het Molengat* (location MG) were analysed further. Ebb measurements contained 15 water samples taken within a time span of 1.5 hours on June 1st, 2022. Flood conditions were captured on May 19th, 2022 and contained 2 water samples taken within 10 minutes. It was assumed that variations in suspended sediment characteristics (particle size, shape, and density) were limited for measurements taken in the same tidal stage but varied between ebb and flood.

The measurements were divided in subsets to assess the performance of the SF and MF method under conditions with 1) little variations in sediment characteristics (ebb measurements); and 2) deviating sediment characteristics (combined ebb and flood measurements).

3.2.2 Colocation of the measurements and determining noise levels

Colocation of the backscatter and water sample reference measurements was based on the time and depth at which the Niskin bottle was closed. First, uncorrected backscatter (R_x) measurements at each frequency were selected for 30 seconds around the moment of closure – approximately the filling time of the bottle – and averaged over 0.50 m around the sampling depth. The final step consisted of time-averaging over the 30 second window. For each reference measurement, noise levels (NT) were determined by averaging R_x over the last 10 cells in each ping (Section 2.1.4) and over the 30 second period.

3.2.3 Echosounder data quality

Data quality of the backscatter measurements was assessed for each frequency. Signal-to-noise ratios (SNR) were determined via:

$$SNR = \frac{R_x}{NT} \tag{24}$$

Obtained values are given in Appendix A. If $SNR < 1.1$, measurements were dropped, which was the case for most 250 kHz data. Hence, further data analysis was carried out for the 1000 and 500 kHz measurements only.

3.2.4 Relative volume backscatter

Correcting for signal losses was done using the sonar equation (Equation 1), though G was not defined as instrument calibration was not performed. Hence, relative volume backscatter (S'_v) measurements were determined with:

$$S'_v = 10\log_{10}\left(10^{\frac{R_x}{10}} - 10^{\frac{NT}{10}}\right) + S_e \tag{25}$$

where the echosounder loss term (S_e) was calculated using the Nortek Signature VM Review software (Equation 2) with absorption loss due to sediment neglected.

3.2.5 Multi-frequency particle size estimations

Estimating particle radii based on backscatter differences between frequencies (ΔS_v) requires calibrated echosounder(s). Because no such calibration was performed on the instrument, ΔS_v was determined with:

$$\Delta S_v = S'_{v,1000\ kHz} - S'_{v,500\ kHz} - \Delta G \tag{26}$$

where ΔG accounts for the difference in unknown echosounder calibration gain parameters for both frequencies. ΔG was optimized by assessing MF SSC estimation results for different values (Appendix C).

By measuring at 1000 and 500 kHz, values of $3.7 < \Delta S_v < 6.0$ and $-1.9 < \Delta S_v < 0$ yielded ambiguous solutions of a_s. For these ranges of ΔS_v, the smallest possible solution of a_s was used in further processing.

Visual observations of the water samples suggested the presence of significant amounts of suspended matter different to sand particles, especially for the ebb samples. Because the form function for quartz sand (Equation 15) was used, the obtained values of a_s are regarded as *equivalent mean particle radii*. For the measured values of ΔS_v, a_s indicates the radius of quartz sand particles that would cause the observed backscatter difference. Comparisons with true mean particle radii were not carried out.

3.2.6 Fitting of backscatter model using the single and multi-frequency method

The SF and MF methods were applied to S'_v measured at 1000 and 500 kHz during ebb (steady sediment characteristics) and ebb and flood combined (varying sediment characteristics). The model fitting parameters (SF: A, B_{SF}; MF: A, B_{MF}, β) were determined using a least-squares algorithm with the colocated reference SSC measurements.

3.2.7 Comparing single and multi-frequency results

Goodness of fit of the obtained backscatter – SSC relations was quantified using correlation coefficients (r^2), root mean square errors (RMSE) and p-values for 1) the relation between measured S'_v and the fitted model (SF: Equation 13; MF: Equation 22) and 2) the rewritten formula in terms of M_s (SF: Equation 14; MF: Equation 23). Using these values, performance of the SF and MF method was assessed and compared under steady (ebb) and varying (ebb and flood) sediment conditions.

4 Results

Results of the field measurements and data analysis are presented in a structure that aligns with the research questions, starting with the results of the single frequency method. Then, the obtained equivalent mean particle radii as part of the MF method are reviewed, followed by the SSC estimation results of that method. Finally in Section 4.4, performance of all fitted backscatter – SSC relations (for SF and MF, applied to 1000 and 500 kHz measurements and for both datasets) is summarized and compared.

4.1 Single frequency method

4.1.1 Ebb measurements

Application of the SF method to the ebb measurements yielded correlation coefficients of $r^2_{1000} = 0.69$ and $RMSE_{1000} = 2.0$ dB for fitting the SF backscatter model (Equation 13) to S'_v measured at 1000 kHz (Figure 10). For the 500 kHz measurements, $r^2_{500} = 0.80$ and $RMSE_{500} = 1.7$ dB (Figure 11).

The underperformance of the 1000 kHz with respect to the 500 kHz measurements is represented in a larger spread in the corresponding scatter plots. For both frequencies, $p \ll 0.05$, indicating significant relations between the measured and modelled backscatter intensities.

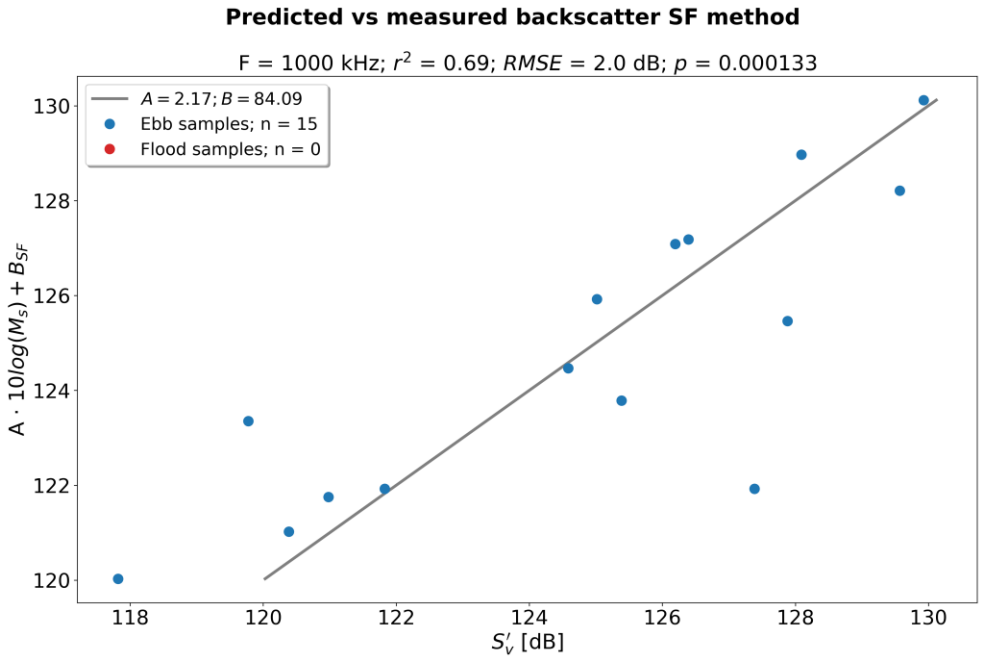

Figure 10: SF backscatter relation fitted to the 1000 kHz ebb measurements.

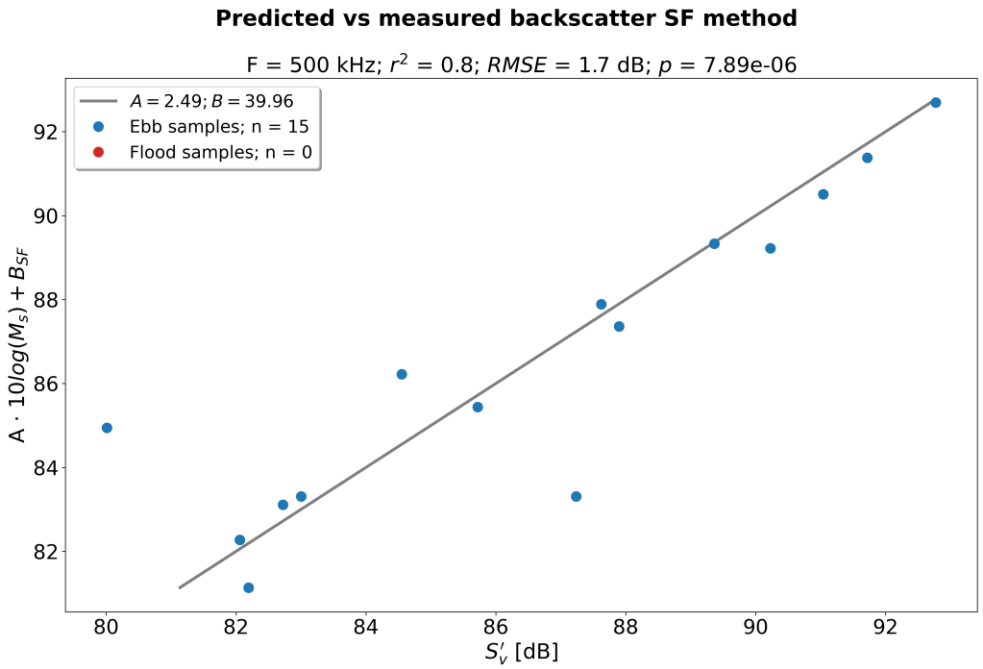

Figure 11: SF backscatter relation fitted to the 500 kHz ebb measurements.

Deriving M_s from the obtained 500 kHz backscatter relation yielded sound results (Figure 12). For most samples, the fitted line was within or not far from the uncertainty range of the reference measurements (grey bars). Figure D. 1 in Appendix D shows the results of the 1000 kHz data.

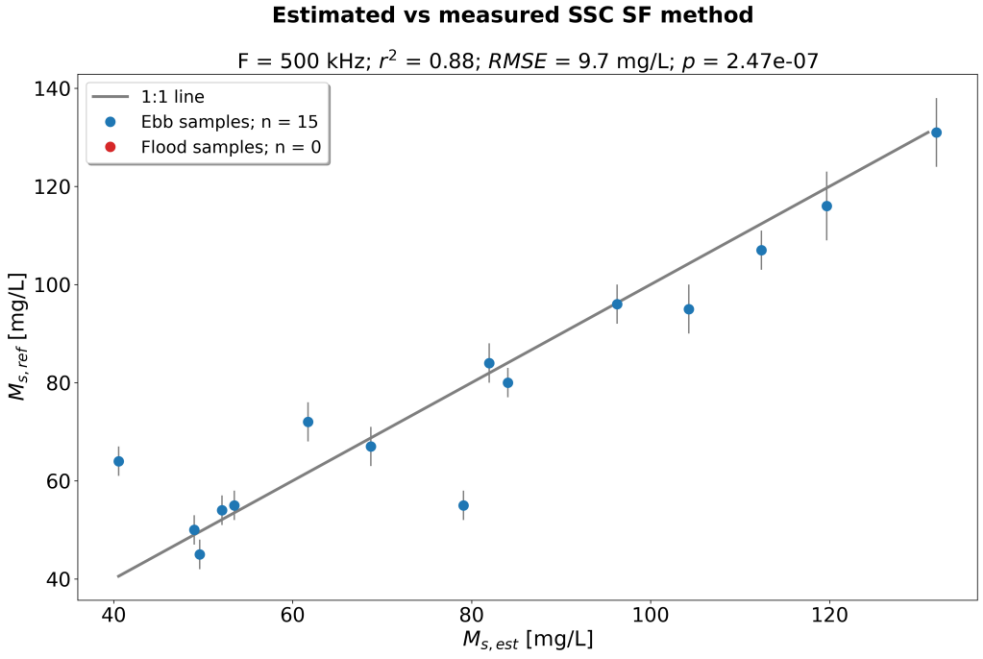

Figure 12: SSC estimations based on the SF backscatter relation fitted to the 500 kHz ebb measurements. The grey bars indicate the uncertainty range of the reference water sample measurements.

4.1.2 Combined ebb and flood measurements

When the SF method was used to fit the backscatter model to the combined ebb and flood measurement set – to assess performance under varying sediment conditions – poor results were obtained for both frequencies: $r^2_{1000} = 0.14$ and $r^2_{500} = 0.41$. $RMSE$s were two times larger than for the ebb only measurements: $RMSE_{1000} = 4.4$ dB; $RMSE_{500} = 3.2$ dB. Obtained p-values suggested a valid relation for the 500 kHz measurements only: $p_{1000} = 0.143 > 0.05$ and $p_{500} = 0.006$. The fitted backscatter relations for the 1000 and 500 kHz measurements are shown in Figure D. 2 and Figure 13 respectively.

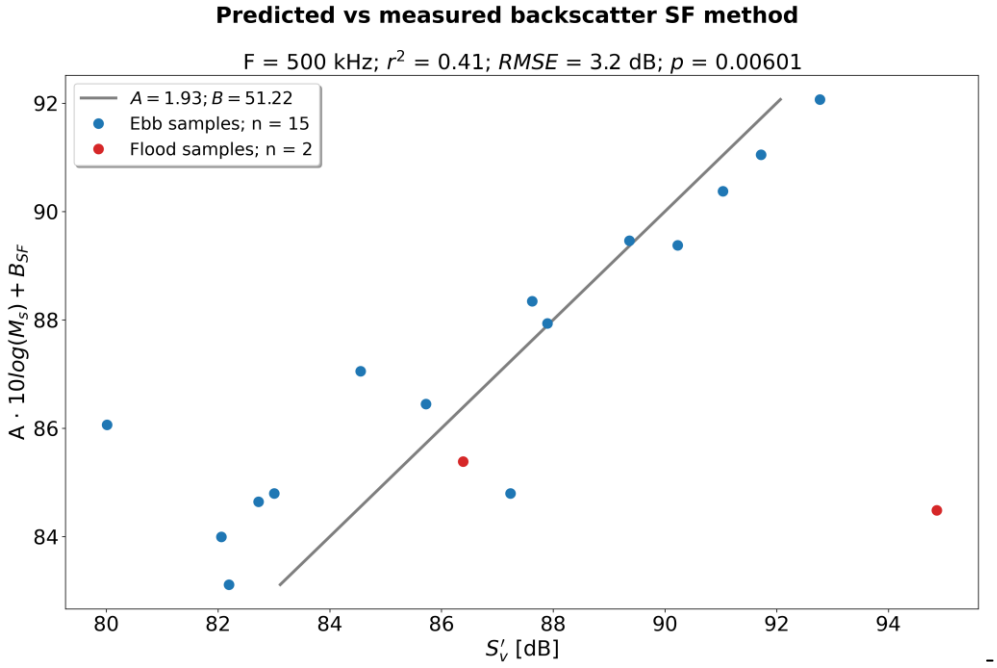

Figure 13: Fitted SF backscatter relation for the combined ebb and flood 500 kHz measurements.

Corresponding SSC estimations indicate significant overestimation of SSC for one of the flood samples (over three times its true value) for the 500 kHz measurements (Figure 14). In addition, precision of the ebb estimates was reduced with respect to when the model was fitted to those measurements only (Figure 12), indicated by a larger spread in data. Worse agreement between echosounder estimated SSC and reference measurements was observed for the 1000 kHz measurements (Figure D. 3).

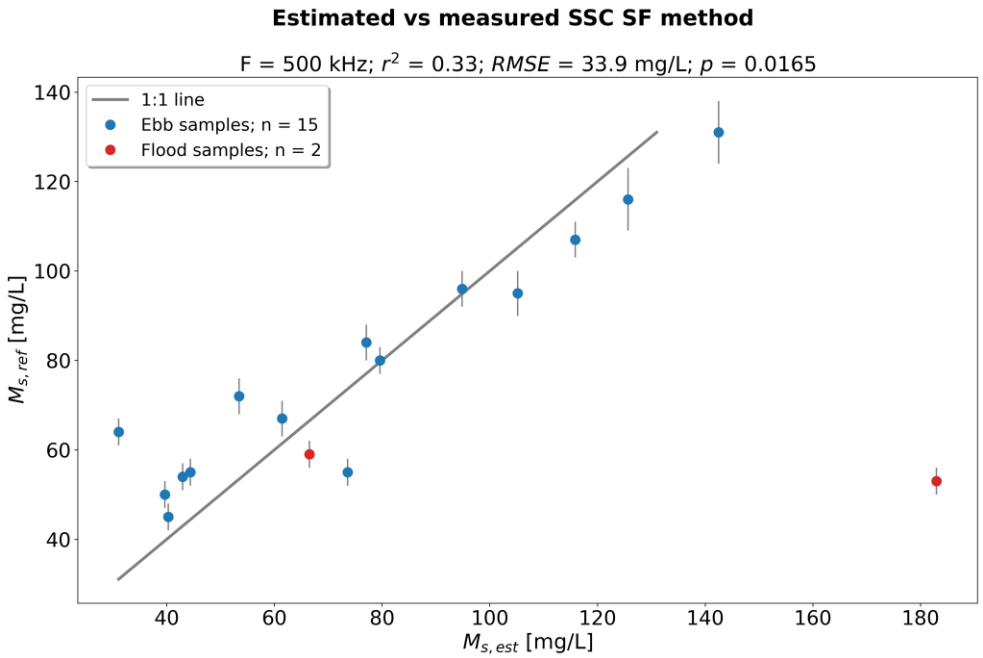

Figure 14: SSC estimations based on the SF backscatter relation fitted to the 500 kHz ebb and flood measurements.

4.2 Derived equivalent particle radii

Based on values of ΔS_v (Table 6), equivalent mean particle radii were derived for the ebb and flood measurements (Figure 15). For the ebb measurements, a_s was in the range of $192 < a_s < 332$ µm, including five samples in the ambiguous region between $3.7 < \Delta S_v < 6.0$ (Figure 15, red circle). From the two available flood samples one was dropped because its value of $\Delta S_v = 12.7$ was outside the resolvable range. For the one remaining flood measurement, $a_s = 81$ µm.

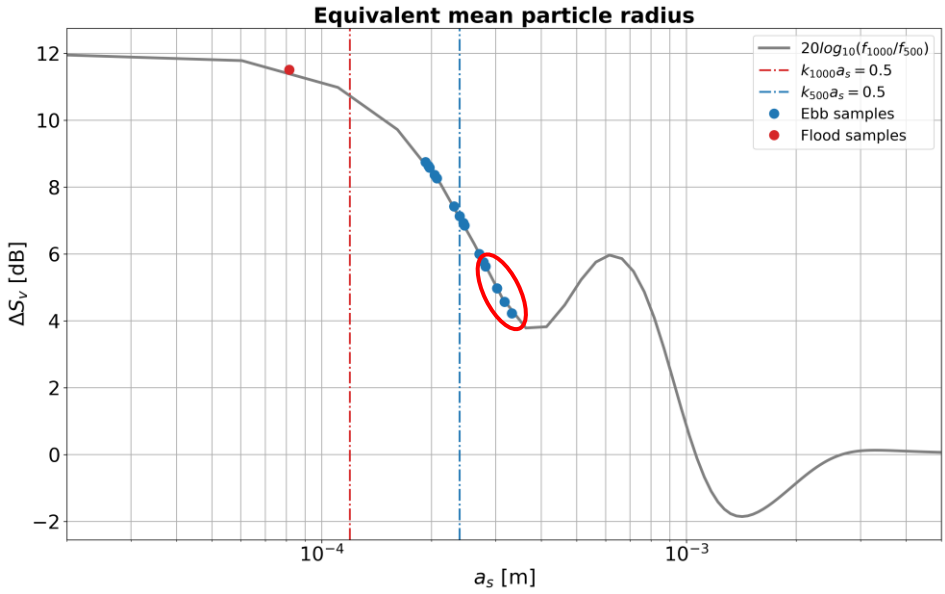

Figure 15: Equivalent mean particle radii based on ΔS_v measurements corresponding to the measurements taken during ebb (blue) and flood (red). Values within the ambiguity region are highlighted in the red circle.

4.3 Multi-frequency method

4.3.1 Ebb measurements

Fitting the backscatter model following the multi-frequency method (Equation 22) to the 1000 and 500 kHz ebb measurements yields similar performance: $r^2_{1000} = 0.78$ and $r^2_{500} = 0.80$; $RMSE_{1000} = RMSE_{500} = 1.7$ dB and $p \ll 0.05$. Corresponding plots of the fitted backscatter relations and derived SSC estimates are in Appendix D.

4.3.2 Combined ebb and flood measurements

Applying the MF method to the combined ebb and flood measurements yielded sound performance relative to the SF results: $r^2_{1000} = 0.88$ and $RMSE_{1000} = 1.7$ dB (Figure 16); $r^2_{500} = 0.68$ and $RMSE_{500} = 2.4$ dB (Figure D. 8). For both frequencies, $p \ll 0.05$. The model successfully accounted for the significantly higher backscatter intensity of the flood measurement, aligning most data points close to the fitted relation.

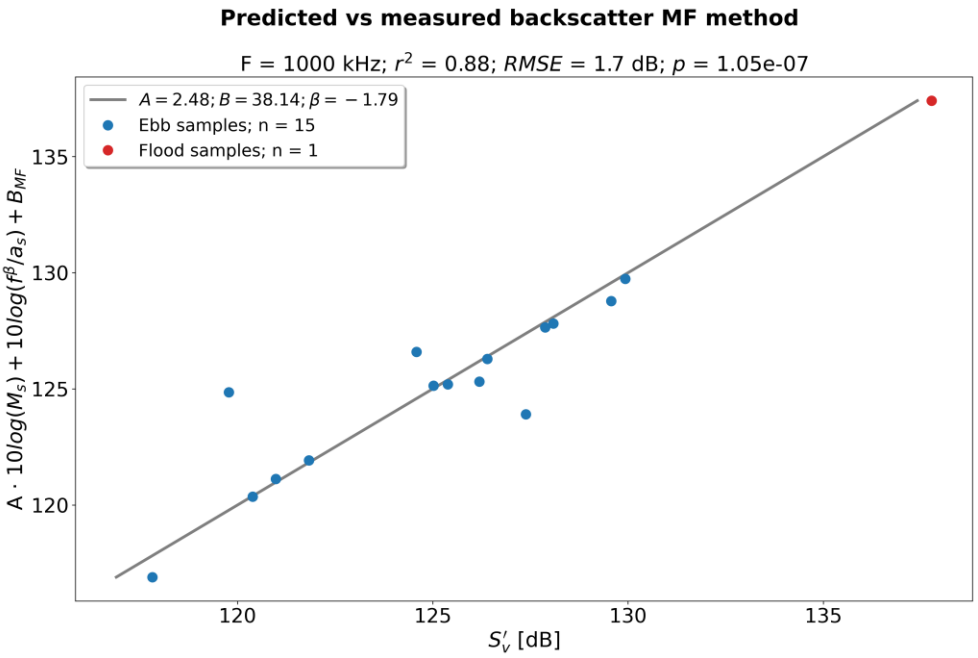

Figure 16: MF backscatter relation fitted to the 1000 kHz ebb and flood measurements.

Derivation of SSC estimates was successful: they showed sound agreement with the reference measurements (Figure 17). The fitted line resided within the error range of most of the reference measurements (grey bars). SSC estimations based on the 500 kHz signal (Figure D. 9) showed slightly poorer agreement with the reference measurements but were significantly improved compared to the SF results.

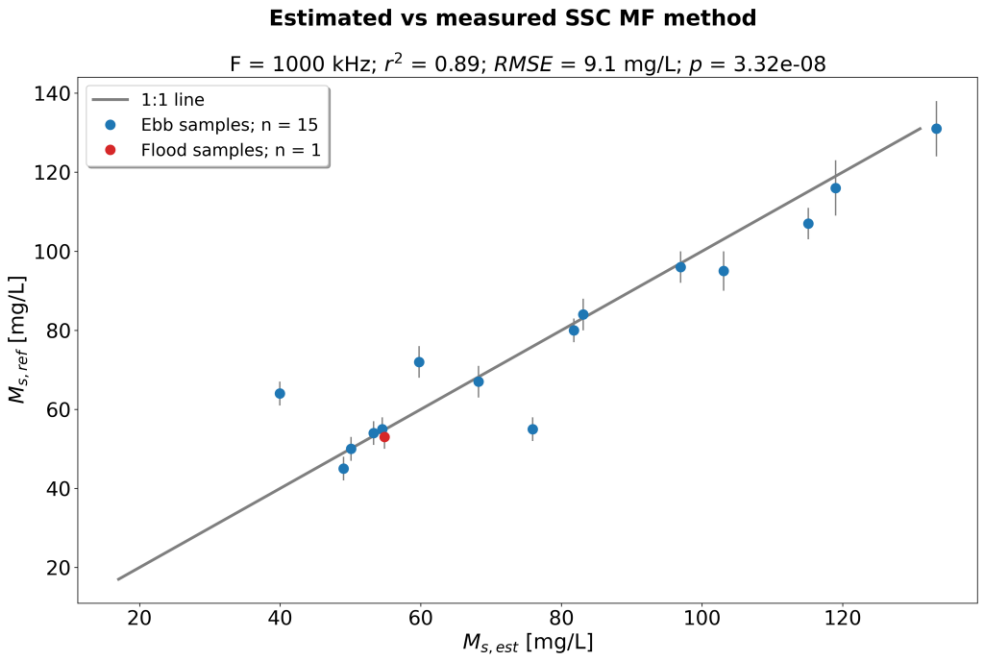

Figure 17: SSC estimations based on the MF backscatter relation fitted to the 1000 kHz ebb and flood measurements.

4.4 Overview of measurements

4.4.1 Fitted backscatter relations

Obtained SF and MF model fitting parameters are given in Table 2 and Table 3 respectively. For all fitted relations, the value of A deviated from the theoretical value ($A = 1$; Section 2.3.1). The values of β also differed from its theoretical value ($\beta = 2$; Equation 22) and were negative, except for the 500 kHz ebb measurements.

	A	B_{SF}
Ebb; 1000 kHz	2.17	84.09
Ebb; 500 kHz	2.49	39.96
Ebb+flood; 1000 kHz	1.29	101.99
Ebb+flood; 500 kHz	1.93	51.22

Table 2: Applied SF fitting parameters.

	A	B_{MF}	β
Ebb; 1000 kHz	2.43	41.04	-1.0
Ebb; 500 kHz	2.42	10.36	0.91
Ebb+flood; 1000 kHz	2.48	38.14	-1.79
Ebb+flood; 500 kHz	2.60	-0.53	-0.45

Table 3: Applied MF fitting parameters.

Main observations of comparing r^2, $RMSE$ and p values include the underperformance of the SF 1000 kHz ebb measurements in relation to the 500 kHz data and the poor results when the SF method was applied to the combined ebb and flood measurement set (Table 4). Both cases were mitigated if the MF method was used.

	1) Ebb measurements					2) Combined ebb + flood measurements				
Method	Figure	*n*	r^2	$RMSE$	p	Figure	*n*	r^2	$RMSE$	p
SF; 1000 kHz	Figure 10	15	0.69	2.0 dB	1.33e-4	Figure D. 2	17	0.14	4.4 dB	0.143
SF; 500 kHz	Figure 11	15	0.80	1.7 dB	7.89e-6	Figure 13	17	0.41	3.2 dB	0.00601
MF; 1000 kHz	Figure D. 4	15	0.78	1.7 dB	1.12e-5	Figure 16	16	0.88	1.7 dB	1.05e-7
MF; 500 kHz	Figure D. 6	15	0.80	1.7 dB	6.84e-6	Figure D. 8	16	0.68	2.4 dB	8.48e-5

Table 4: Fitting performance of backscatter models.

4.4.2 SSC estimation performance

Results of rewriting the fitted backscatter models (Table 4) in terms of M_s (SF: Equation 14; MF: Equation 23) agree with these observations: underperformance of the SF method applied to the 1000 kHz relative to the 500 kHz ebb measurements; poor SF performance for the combined ebb and flood measurement sets and improved results following the MF method in these cases (Table 5).

	1) Ebb measurements					2) Combined ebb + flood measurements				
Method	Figure	*n*	r^2	$RMSE$	p	Figure	*n*	r^2	$RMSE$	p
SF; 1000 kHz	Figure D. 1	15	0.70	15.6 mg/L	1.03e-4	Figure D. 3	17	0.00	138.6 mg/L	0.959
SF; 500 kHz	Figure 12	15	0.88	9.7 mg/L	2.47e-7	Figure 14	17	0.33	33.9 mg/L	0.0165
MF; 1000 kHz	Figure D. 5	15	0.87	9.8 mg/L	3.15e-7	Figure 17	16	0.89	9.1 mg/L	3.32e-8
MF; 500 kHz	Figure D. 7	15	0.86	10.2 mg/L	5.60e-7	Figure D. 9	16	0.82	13.3 mg/L	1.33e-6

Table 5: Performance of SSC estimations.

4.4.3 Backscatter intensities, derived particle radii and concentrations

Measured backscatter intensities, corresponding values of ΔS_v, derived values of a_s ($a_{s,1}$ and $a_{s,2}$ indicating ambiguous values) and ka_s for both frequencies, SSC estimations ($M_{s,est}$) and reference measurements including their absolute error ($M_{s,ref}$) were summarized (Table 6). Here, $M_{s,est}$ was based on the combined ebb and flood dataset measured at 500 kHz (SF method) and 1000 kHz (MF method).

As explained earlier, the SF method yielded an SSC value of one of the flood samples that was more than three times the reference value. Only two values are within the uncertainty range of the reference measurements whereas for the MF method, most measurements are – including the flood sample.

#	Tide	$S'_{v,1000}$ [dB]	$S'_{v,500}$ [dB]	ΔS_v [dB]	a_s [µm]	$a_{s,1}$ [µm]	$a_{s,2}$ [µm]	$k_{1000}a_s$ [µm]	$k_{500}a_s$ [µm]	$M_{s,ref}$ [mg/L]	$M_{s,est}$ (SF) [mg/L]	$M_{s,est}$ (MF) [mg/L]
1	flood	137.8	94.9	11.5	81	-	-	0.34	0.17	53 ±3	183	55
2	flood	130.5	86.4	12.7	-	-	-	-	-	59 ±3	66	-
3	ebb	127.4	87.2	8.7	192	-	-	0.80	0.40	55 ±3	74	76
4	ebb	125.4	85.7	8.3	207	-	-	0.86	0.43	67 ±4	61	68
5	ebb	124.6	84.6	8.6	196	-	-	0.82	0.41	72 ±4	53	60
6	ebb	127.9	87.9	8.6	197	-	-	0.83	0.41	80 ±3	80	82
7	ebb	129.6	91.0	7.1	239	-	-	1.00	0.50	107 ±4	116	115
8	ebb	126.4	89.4	5.6	281	549	699	1.18	0.59	96 ±4	95	97
9	ebb	121.8	83.0	7.4	231	-	-	0.96	0.48	55 ±3	44	55
10	ebb	119.8	80.0	8.4	204	-	-	0.85	0.43	64 ±3	31	40
11	ebb	125.0	87.6	6.0	271	-	-	1.13	0.57	84 ±4	77	83
12	ebb	121.0	82.7	6.9	246	-	-	1.03	0.52	54 ±3	43	53
13	ebb	117.8	82.2	4.2	332	447	808	1.39	0.69	45 ±3	40	49
14	ebb	129.9	92.8	5.8	278	564	683	1.16	0.58	131 ±7	142	133
15	ebb	128.1	91.7	5.0	302	496	759	1.26	0.63	116 ±7	126	119
16	ebb	126.2	90.2	4.6	317	470	787	1.33	0.66	95 ±5	105	103
17	ebb	120.4	82.1	6.9	244	-	-	1.02	0.51	50 ±3	40	50

Table 6: Overview of measurement results including backscatter intensities, derived equivalent particle radii and corresponding values of ka_s, reference SSC measurements and estimated values based on the SF and MF method for the combined ebb and flood measurement set.

5 Discussion

Here, results and performance of the SF and MF methods in fitting the general backscatter model to the S_v' measurements are discussed, including some remarks about the certainty of the measurement approach and validity of obtained particle radius estimations.

5.1 General remarks

5.1.1 Model fitting parameters

The fitting parameter A was introduced in the SF and MF method to fit the general backscatter model to reference SSC measurements. According to the theory, backscatter intensities are related to SSC via $S_v \sim \log_{10}(M_s)$ (Equation 10) and the backscatter – SSC relation would follow a 1:1 slope, with SSC on the logarithmic domain. However, the results suggest observed backscatter intensities were related to SSC through $S_v \sim A \cdot \log_{10}(M_s) = \log_{10}(M_s^A)$ where the slope of the relation, A, would range between 1.3 and 2.6 (Table 2 and Table 3).

Varying values of B_{SF} and B_{MF} were obtained. If a calibrated echosounder was used, B_{MF} would be equal to K_2 and account for variations in particle shape and density. However, no instrument calibration was carried out and there is an unknown contribution of G_{1000} and G_{500} in B_{MF}.

Regarding the MF method, if $\beta \neq 2$, the behaviour of measured backscatter intensities deviates from the theoretical behaviour described by the model (Equation 11). This was the case for all measurements, with negative values for most obtained relations (Table 3). Possibly, this deviation originated from the form function not being representative of the actual suspended sediment (Section 5.3.2).

5.1.2 Measurement uncertainty

Measurement uncertainty must be considered when statements about performance of both methods are made. The limited amount of reference measurements obtained – 15 ebb and 2 flood samples – must therefore be taken into account. This especially applies to the flood data, since one sample was not included in the MF method because its ΔS_v value was outside the resolvable range. In addition, processing of the flood samples deviated slightly from the ebb measurements – a different sieve size was used to separate fine and coarse material, and some additional steps were included during lab processing (Appendix B) – potentially affecting the accuracy of the reference measurements.

For these reasons, it is recommended that more field measurements are conducted for extended periods in future research to increase certainty in assessing performance differences between the SF and MF methods.

5.2 Performance differences

5.2.1 Single frequency method – between frequencies

For both measurement sets, lower performance was obtained when the SF method was applied to the 1000 kHz measurements than for those obtained at 500 kHz. Based on ka_s values, it can be concluded that the 1000 kHz measurements were in the interferential regime because for all ebb measurements, $k_{1000}a_s \approx 1$ (Table 6). For the 500 kHz ebb measurements, $k_{500}a_s \approx 0.5$, indicating measurements around the upper boundary of the Rayleigh regime.

Based on this, taking measurements at a frequency of 500 kHz or lower – to steer away from the Rayleigh regime boundary – would lead to improved SSC estimations for the type of suspended particles that were present during the ebb measurements.

For the flood measurement where a_s was successfully estimated, $ka_s < 0.5$ for both signals. In theory, this indicates that for the sediment characteristics of that measurement, a 1000 kHz signal would also lead to sound SSC estimations – if there are no major variations in particle properties.

5.2.2 Single frequency method – between measurement sets

The SF method was expected to yield good results only when there is little change in suspended sediment characteristics (particle size, shape and density; Section 1.2.3) due to parameters K_1 and K_2 not being resolved (Equation 10).

Based on the assumption that particle properties varied between ebb and flood, it can be concluded that this statement was confirmed with the field measurements. While the SF method (at 500 kHz) yielded sound results for the ebb only measurements, performance was significantly dropped when it was applied to the combined ebb and flood measurement set. Hence, for the SF method to be successful over various tidal stages, reference measurements should be taken frequently to readjust the model fitting parameters (A; B_{SF}) to the temporally varying sediment characteristics.

The assumption of varying particle properties was partly validated with the derived equivalent mean particle radii: significantly larger values of a_s were obtained for the ebb compared to the flood measurement(s).

5.2.3 Multi-frequency method – between frequencies

Performance differences were observed when the MF method was applied to the 1000 and 500 kHz data (Table 4). This contrasted with theory, because differences in backscattering behaviour based on particle size and frequency should be compensated for by parameter K_1 (Equation 11) and fitted backscatter relations should yield identical values of M_s for backscatter data independent of acoustic frequency. Not fulfilling the assumptions introduced in the derivation of a_s (Section 5.3.2) could be a potential cause in this.

5.3 Equivalent particle radii

5.3.1 Lack of echosounder calibration

A value of $\Delta G = 31.4$ dB was applied to compensate for the absence of instrument calibration data to determine ΔS_v for each measurement. Selection of this value led to sound performance in estimating SSC using the MF method, but a sensitivity analysis showed that application of $\Delta G = 31.0$ dB would have yielded slightly increased performance of the 500 kHz measurements (Appendix C). In future work, it is recommended to calibrate the echosounder at each frequency to eliminate assumptions regarding ΔG and to increase certainty in a_s derivations. However, the sensitivity of MF SSC estimation performance to the choice of ΔG was found to be limited (Table C. 1), presumably due to the method's capability of compensating for inaccurate a_s estimations through the model fitting parameters A, B_{MF} and β.

5.3.2 Validity of applied form function

The derived values of a_s are measured in terms of *equivalent mean particle radii*, indicating particle radii that would apply to quartz sand particles based on the measured values of ΔS_v. No comparisons with true particle radii were conducted, however visual observations of the water samples indicated the presence of significant amounts of material different to sand particles (Figure 18). Hence, the applicability of the used quartz sand form function may be limited. This also applies to the assumption of the particle sizes to be narrowly distributed.

Further studying of the applicability of form functions by comparison with actual sediment characteristics can increase certainty in the process of deriving particle radii from multi-frequency backscatter differences.

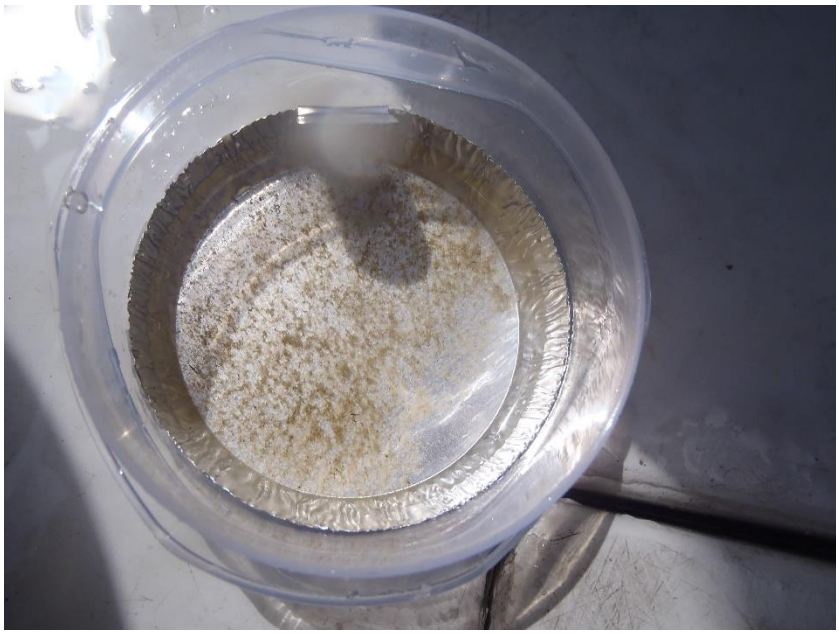

Figure 18: Coarse material that remained on the sieve for one of the ebb samples. Although not further analysed, visual observations indicated presence of significant amounts of material different to sand – possibly organic material or flocs.

5.3.3 Resolvable range

Limitations in the range of a_s that can be resolved were observed for one of the flood samples, where its value of $\Delta S_v = 12.7$ dB exceeded the upper boundary of the form function ratio based on the 1000 and 500 kHz frequency set. This may have been the result of measurement error, where the recorded S_v' value of at least one of the frequencies could be regarded as an outlier. Another potential cause would be limited sensitivity of the 500 kHz signal due to the particles being very small in relation to the wavelength, therefore not meeting the $ka_s > 0.05$ criterion. Lastly, application of a larger value of ΔG would have reduced the observed difference in backscatter so that ΔS_v would reside in the resolvable range, but would also lead to significantly lower SSC estimation performance of the MF method (Figure C. 1 and Table C. 1).

For the ΔS_v data in the ambiguity range of the form function ratio, a_s was assumed to equal the lowest of the three possible solutions, but no validation against true values was conducted.

Using frequencies that are further apart, e.g. 1000 and 250 kHz, overcomes the ambiguity region in the solution of a_s (Section 2.4.2). For future applications, the instrument needs to be adapted to improve the signal strength of 250 kHz measurements.

5.4 Potential of single instrument, multi-frequency ADCP echosounder measurements

Current SF methods require auxiliary measurements to account for varying backscatter behaviour due to variations in particle size, shape and density. For example in Cutroneo et al. (2014), single frequency ADCP backscatter measurements were combined with OBS measurements to track dredge plumes. In Fromant et al. (2022), a multi-frequency ABS instrument was lowered into the ensonified volume of single frequency multibeam backscatter measurements at distinct time intervals to obtain particle size estimates in efforts to improve sediment characterization over the water column.

For the MF method, reference measurements are still required to adapt the backscatter model to the nature (particle shape and density) of the sediment. But because of the ability to adjust for variations in particle size, it is expected that under changing conditions not covered by reference measurements, relatively sound SSC estimations can be obtained. MF echosounder ADCP measurements could be taken using stationary bottom or buoy mounted setups, or in moving boat setups as was done in this research. Relative to SSC measurements using water samples or optical instruments, significantly higher temporal and spatial resolutions can be captured.

If further research is carried out in validating particle size estimations (increased statistical validation, use of a form function applicable to the actual type of sediment and use of a calibrated instrument), sediment fluxes can be characterised based on particle size estimations and flow velocity measurements.

5.4.1 Turbidity monitoring

The use of MF ADCP measurements can be of great potential for monitoring of dredge plumes. Due to the variety in particle sizes present in dredge plumes, SF methods would struggle in retaining high SSC estimation performance, whereas the MF method is expected to yield better results. Particle size estimations could be used to distinguish varying types of suspended particles such as stirred-up bed aggregates and finer floc-forming matter suspended in the water column. Because 3D flow structures are measured with ADCPs, it would be possible to capture complex suspended sediment transport processes present in dredge plumes, which can be a source in improving numerical models.

6 Conclusions

Acoustical instruments, including ADCPs, are used to capture suspended sediment processes in coastal research and to monitor turbidity plumes during dredging. They have potential to overcome challenges of alternative methods which are labour-intensive and have limited measurement range, and therefore poor spatial and temporal resolutions. However, single frequency (SF) measurements involve limitations in the range of sediment characteristics that can be resolved which in practise leads to the requirement of frequent acquiring of reference measurements.

Multi-frequency (MF) measurements are used to reduce the sensitivity to changing sediment characteristics, and studies have been conducted using separate instruments measuring at distinct frequencies. The development of a single ADCP, capable of taking high-resolution echosounder measurements at multiple frequencies has allowed an exploration of the following question:

What is the added value of single instrument, multi-frequency echosounder measurements in quantifying suspended sediment compared to single frequency measurements?

The work has been based around sub-questions (Section 1.4) for which concluding answers are formulated in this section.

6.1 Single frequency echosounder SSC estimations

The first sub-question was stated as:

Under what conditions can SSC successfully be estimated using single frequency echosounder measurements and what are the limitations of the method?

6.1.1 Theoretical method applicability

To assess the performance of the SF method and its limitations, the general model that relates acoustic backscatter to sediment properties was first introduced in Section 2.2. Based on this model, the backscatter intensity is coupled to 1) the concentration of the particles; 2) the mean particle size and 3) their shape and density. When SF echosounder measurements are taken, the model can be used to solve for SSC if the characteristics of the particles being measured are consistent, and reference SSC measurements are used to tune the model to the specific sediment properties.

For SF measurements, optimal results are obtained when the transmitted wavelength is much larger than the radius of the particles being measured. Then, backscatter is in the Rayleigh regime, and the product of the acoustic wavenumber and particle radius product (ka_s) is much smaller than one (for quartz sand particles, $ka_s < 0.5$ applies). For sufficient sensitivity, $ka_s > 0.05$ is suggested as a lower bound (Lohrmann, 2001). If $0.5 < ka_s < 5$, the particle radius is on the same order as the wavelength, causing unpredictable backscatter intensities due to interference (the interferential scattering regime). For $ka_s > 5$, the geometric scattering regime applies, and the backscatter response becomes independent of particle size and wavelength. Due to this relation, the optimal frequency to measure SSC varies between conditions with deviating particle size ranges.

6.1.2 Field measurements

Observations based on the field measurements taken around Texel support these relationships. To sample relatively consistent sediment properties, measurements were taken at the same location within a short time span of 1.5 hours (ebb dataset) and yielded sound performance of the SF echosounder SSC estimations: $r^2_{1000\ kHz} = 0.70$ and $r^2_{500\ kHz} = 0.88$. Observed values of ka_s – where a_s indicated the equivalent mean radius linked to quartz sand particles – show that superior correlations with the 500 kHz dataset was attributed to a more optimal wavelength-particle size relationship; particles resided in the Rayleigh regime of the 500 kHz measurements and in the interferential regime of the 1000 kHz measurements.

Measurements were taken at 250 kHz as well, but signal strengths were insufficient due to poor transducer performance at that frequency. Hence, the 250 kHz measurements were disregarded, and adaptation of the instrument is suggested for future applications.

Fitting the backscatter model to the reference measurements of the combined ebb and flood measurement set yielded poor performance of the SSC estimations: $r^2_{1000\ kHz} = 0.00$ and $r^2_{500\ kHz} = 0.33$ with accompanying large values of $RMSE$. Based on the assumption that the sediment properties at the measurement site differed between ebb and flood, it can be stated that SSC can successfully be estimated using the SF method only under conditions where there is little variation in characteristics of the suspended sediment and sufficient reference measurements are available.

6.2 Multi-frequency echosounder particle size estimations

The second sub-question regarded the estimation of particle size as part of the MF method:

How can mean particle size be derived from multi-frequency echosounder measurements?

6.2.1 Acoustic frequency – particle radius relation

Backscatter intensities depend on the product of the acoustic wavenumber and the radius of the particles on which the signal is reflected, ka_s. Because the wavenumber is determined by the acoustic frequency F, it follows that when measuring at a certain acoustic frequency, the measured backscatter intensity will vary for particles of different size. It also means that when measuring at multiple frequencies, different backscatter intensities will be recorded for each frequency capturing the same cloud of sediment. This relation of ka_s can be described in a form function (f) based on lab measurements, for example for quartz sand (Equation 15).

If the echosounder is calibrated, measurements in terms of absolute volume backscatter (S_v) are obtained. Then, the difference in backscatter measured at two frequencies (ΔS_v) is linked to the ratio of the form function evaluated at each frequency (Equation 20). From this the mean particle radius can be derived directly, assuming that the particle sizes are narrowly distributed and the applied form function is sufficiently representative of the actual sediment backscattering behaviour.

6.2.2 Resolvable range

The resolvable range of the estimated particle radii depends on the selection of acoustic frequencies. The highest frequency determines the smallest particles for which a_s can be resolved, whereas the largest resolvable a_s is dictated by the lowest frequency (Figure 4).

The interval between F_1 and F_2 should be large enough to overcome ambiguity in the solution of a_s. In addition, larger frequency intervals allow for increased precision because a change in a_s is related to a larger step in ΔS_v. Because S_v is measured at each frequency with a set precision, this implies that the error in a_s is reduced since the relative error in ΔS_v is smaller.

6.2.3 Field measurements

In the process of deriving particle radius estimations from measured backscatter differences, the form function of quartz sand particles (Equation 15) was used. However, visual observations of the water samples suggested the presence of particles of different nature. Besides, assumptions were made regarding echosounder calibration values through ΔG. Because no assessment was made with reference measurements, the accuracy of the particle radius estimations was not validated.

6.3 Multi-frequency echosounder SSC estimations

To what extend does the multi-frequency method overcome the limitations of the single frequency method?

6.3.1 The MF method

The MF method solves the general backscatter model (Equation 10) not only for SSC, but particle size as well, based on differences in backscatter intensity at each frequency. Using the model, SSC can be derived directly under the assumption that the particles are spherical, of uniform density and follow a narrow PSD (Equation 13). The form function should be sufficiently representative of the sediment backscattering behaviour and the echosounder should be calibrated. In theory, reference measurements would not be required, and SSC could be estimated under conditions with varying particle sizes if the above-mentioned conditions are met. In addition, performance of SSC estimations becomes less dependent on acoustic frequency because the model compensates for variations in backscattering behaviour, including measurements that are in the interferential regime. However, the acoustic frequencies must be chosen in consideration of the range of particle radii that can be resolved (Section 6.2.2).

Validity of all mentioned assumptions rarely occurs. Suspended matter often has varying densities and shapes, leading to deviations from the backscattering behaviour described by the model. To account for this varying behaviour, fitting parameters (A, B and β) were introduced. As with the SF method, the model can be tuned to specific suspended sediment characteristics using reference SSC measurements. While the SF method only performs well under conditions with uniform sediment characteristics, the MF method is expected to retain performance better since it accounts for variations in particle size.

6.3.2 Field measurements

The MF method was applied to the same measurement sets as the SF method: one containing only measurements taken during ebb, the other also including flood measurements. In the first case, performance was comparable to the 500 kHz SF estimations. In comparison to the 1000 kHz SF estimations, performance was increased ($r^2_{1000\ kHz,SF} = 0.70$; $r^2_{1000\ kHz,MF} = 0.87$) which demonstrated the method's ability to compensate for the sensitive backscattering behaviour in the interferential regime.

The MF method also performed well with the combined ebb and flood measurement set. The fitting parameters were successfully determined to describe the backscattering behaviour of the particles during both tidal stages. Where SSC was significantly overestimated for the flood samples with the SF method, sound results were obtained with the MF method: $r^2_{1000\ kHz,MF} = 0.89$; $r^2_{500\ kHz,MF} = 0.82$. This suggests that the dependency on reference measurements to account for varying sediment characteristics is significantly reduced, but the limited amount of reference measurements taken during flood must be considered regarding the certainty of this statement.

6.4 Main research question

The focus of this research has been on assessing the performance of the MF method in estimating SSC under varying measurement conditions. The SF method showed limited skill with combined ebb and flood data. This implied that to obtain accurate SF SSC estimations during varying tidal stages, frequent redetermining of the model fitting parameters is required by taking reference measurements. In addition, performance is dependent on the selection of acoustic frequency in consideration of the size of the particles.

Applying the MF method showed that reference measurements were still required to adapt to the specific nature of the particles and to overcome the lack of an instrument calibration. The obtained performance was less specific to the frequency on which the backscatter model was solved in comparison to the SF method. However, the range of particle radii that can be resolved is governed by the selection of acoustic frequencies for which consideration of the expected particle size is still required.

Although further research is required to validate derived particle radius estimations and to obtain further statistical validation of SSC estimation performance, single instrument, multi-frequency ADCP echosounder measurements show potential in improving SSC estimations under varying sediment conditions, which can be a valuable source in characterizing sediment fluxes in coastal research and monitoring of sediment plumes during dredging operations.

6.5 Recommendations

6.5.1 Improving the 250 kHz signal strength

To overcome the ambiguity in particle radii estimations, it is suggested to measure backscatter at frequencies that are further apart than the 1000 and 500 kHz signals used in this research. Although the instrument was configured to measure at 250 kHz as well, data quality was poor, likely due to incompatibility between the 250 kHz signal and a transducer that was designed for 1000 kHz. If obtained SNRs were higher, a_s could be derived without ambiguity. In addition, if backscatter is measured at 3 frequencies, a_s can be estimated based on three form function ratios, increasing measurement certainty.

6.5.2 Instrument calibration

A vital step in obtaining accurate particle radius estimations is the calibration of the echosounder at each acoustic frequency. This way, a_s can be derived directly from ΔS_v and unlike the methodology used in this report, no assumptions on ΔG must be made.

6.5.3 Further statistical validation

After performing the preceding steps, further validation of the method is recommended by obtaining a larger set of reference measurements over a range of varying conditions. This way, more certainty in the performance of the method can be obtained.

6.5.4 Further research form function

To advance the potential of suspended particle characterization using multi-frequency measurements, research efforts should be put into analysing form functions for particles other than quartz sand.

References

Aquatec. (2018). AQUAscat 1000 Buyer's Guide. In.

Bartholomä, A., Kubicki, A., Badewien, T. H., & Flemming, B. W. (2009). Suspended sediment transport in the German Wadden Sea—seasonal variations and extreme events. *Ocean Dynamics*, *59*(2), 213-225. https://doi.org/10.1007/s10236-009-0193-6

Cleveringa, J. (2001). Zand voor zuidwest Texel: Technisch advies RIKZ over vier mogelijke ingrepen in het Zeegat van Texel. *Rapportnr.: OS/2001.031*.

Crawford, A. M., & Hay, A. E. (1993). Determining suspended sand size and concentration from multifrequency acoustic backscatter. *The Journal of the Acoustical Society of America*, *94*. https://doi.org/10.1121/1.407237

Cutroneo, L., Castellano, M., Pieracci, A., Povero, P., Tucci, S., & Capello, M. (2014). The use of a combined monitoring system for following a turbid plume generated by dredging activities in a port. *Journal of Soils and Sediments*, *12*, 797-809. https://doi.org/10.1007/s11368-012-0486-0

Deines, K. L. (1999, 13-13 March 1999). Backscatter estimation using Broadband acoustic Doppler current profilers. Proceedings of the IEEE Sixth Working Conference on Current Measurement (Cat. No.99CH36331),

Demer, D. A., Berger, L., Bernasconi, M., Bethke, E., Boswell, K., Chu, D., Domokos, R., Dunford, A., Fassler, S., Gauthier, S., Hufnagle, L. T., Jech, J. M., Bouffant, N., Lebourges-Dhaussy, A., Lurton, X., Macaulay, G. J., Perrot, Y., Ryan, T., Parker-Stetter, S., . . . Williamson, N. (2015). Calibration of acoustic instruments. *ICES Cooperative Research Report*, *326*.

Echoview. (2022). Echoview learner guide - Fundamentals. In.

Floc'H, F., Ingouf, C., Jourdin, F., Daly, C., Almeida, L. P., Detantd, G., & Almar, R. (2019). *Dual Frequency Acoustic Measurements of Turbulence and Sedimentary Flows* Coastal Sediments 2019,

Fordeyn, J., Lemey, E., & Perk, L. (2020). A holistic approach to coastal protection for the Prins Hendrik Polder. *Hydrolink*.

Fromant, G., Le Dantec, N., & Floc'H, F. (2022). Mapping Water Column Content During Bathymetry Surveys. *Hydro International*.

Gartner, J. W. (2004). Estimating suspended solids concentrations from backscatter intensity measured by acoustic Doppler current profiler in San Francisco Bay, California. *Marine Geology*, *211*(3), 169-187. https://doi.org/https://doi.org/10.1016/j.margeo.2004.07.001

Gartner, J. W., Cheng, R. T., Wang, P.-F., & Richter, K. (2001). Laboratory and field evaluations of the LISST-100 instrument for suspended particle size determinations. *Marine Geology*, *175*(1), 199-219. https://doi.org/https://doi.org/10.1016/S0025-3227(01)00137-2

Gray, J. R., & Gartner, J. W. (2009). Technological advances in suspended-sediment surrogate monitoring. *Water Resources Research*, *45*(4). https://doi.org/10.1029/2008wr007063

Guerrero, M., Rüther, N., & Szupiany, R. N. (2012). Laboratory validation of acoustic Doppler current profiler (ADCP) techniques for suspended sediment investigations. *Flow Measurement and Instrumentation*, *23*(1), 40-48. https://doi.org/https://doi.org/10.1016/j.flowmeasinst.2011.10.003

Guerrero, M., Szupiany, R. N., & Latosinski, F. (2013). Multi-frequency acoustics for suspended sediment studies: an application in the Parana River. *Journal of Hydraulic Research*, *51*(6), 696-707. https://doi.org/10.1080/00221686.2013.849296

Hay, A. E. (1991). Sound scattering from a particle-laden, turbulent jet. *The Journal of the Acoustical Society of America*, *90*(4), 2055-2074. https://doi.org/10.1121/1.401633

Hay, A. E., & Sheng, J. (1992). Vertical profiles of suspended sand concentration and size from multifrequency acoustic backscatter. *Journal of Geophysical Research*, *97*(C10). https://doi.org/10.1029/92jc01240

He, C., & Hay, A. E. (1993). Broadband measurements of the acoustic backscatter cross section of sand particles in suspension. *The Journal of the Acoustical Society of America*, *94*(4), 2247-2254. https://doi.org/10.1121/1.407496

Hoitink, A. J. F., & Hoekstra, P. (2005). Observations of suspended sediment from ADCP and OBS measurements in a mud-dominated environment. *Coastal Engineering*, *52*(2), 103-118. https://doi.org/10.1016/j.coastaleng.2004.09.005

Jourdin, F., Tessier, C., Le Hir, P., Verney, R., Lunven, M., Loyer, S., Lusven, A., Filipot, J.-F., & Lepesqueur, J. (2014). Dual-frequency ADCPs measuring turbidity. *Geo-Marine Letters*. https://doi.org/10.1007/s00367-014-0366-2

Kim, Y. H., & Voulgaris, G. (2003). Estimation of suspended sediment concentration in estuarine environments using acoustic backscatter from an ADCP. Proceedings of Coastal Sediments,

Lohrmann, A. (2001). Monitoring Sediment Concentration with acoustic backscattering instruments. *Nortek Technical Note*.

Medwin, H., & Clay, C. S. (1998). *Fundamentals of acoustical oceanography*. Elsevier.

Merckelbach, L. M., & Ridderinkhof, H. (2005). Estimating suspended sediment concentration using backscatterance from an acoustic Doppler profiling current meter at a site with strong tidal currents. *Ocean Dynamics*, *56*(3-4), 153-168. https://doi.org/10.1007/s10236-005-0036-z

Moore, S. A., Coz, J. L., Hurther, D., & Paquier, A. (2013). Using multi-frequency acoustic attenuation to monitor grain size and concentration of suspended sediment in rivers. *The Journal of the Acoustical Society of America*, *133*(4), 1959-1970. https://doi.org/10.1121/1.4792645

Nortek. (2020). *Webinar: How to use ADCPs to estimate suspended sediment properly*.

Nortek. (2022a). *Echosounder Correction*.

Nortek. (2022b). *Principles of Operation Signature* [Technical documentation].

Nortek. (2022c). Signature 1000 Technical Documentation. In.

Pearson, S. G., Verney, R., Prooijen, B. C., Tran, D., Hendriks, E. C. M., Jacquet, M., & Wang, Z. B. (2021). Characterizing the Composition of Sand and Mud Suspensions in Coastal and Estuarine Environments Using Combined Optical and Acoustic Measurements. *Journal of Geophysical Research: Oceans*, *126*(7). https://doi.org/10.1029/2021jc017354

Reichel, G., & Nachtnebel, H. P. (1994). Suspended sediment monitoring in a fluvial environment: Advantages and limitations applying an Acoustic Doppler Current Profiler. *Water Research*, *28*(4), 751-761. https://doi.org/https://doi.org/10.1016/0043-1354(94)90083-3

Sassi, M. G., Hoitink, A. J. F., & Vermeulen, B. (2012). Impact of sound attenuation by suspended sediment on ADCP backscatter calibrations. *Water Resources Research*, *48*(9). https://doi.org/https://doi.org/10.1029/2012WR012008

Schulkin, M., & Marsh, H. W. (1962). Sound Absorption in Sea Water. *The Journal of the Acoustical Society of America*, *34*(6), 864-865. https://doi.org/10.1121/1.1918213

Simmons, S., Parsons, D., Best, J., Orfeo, O., Lane, S., Kostaschuk, R., Hardy, R., West, G., Malzone, C., Marcus, J., & Pocwiardowski, P. (2010). Monitoring Suspended Sediment Dynamics Using MBES. *Journal of Hydraulic Engineering*, *136*. https://doi.org/10.1061/(ASCE)HY.1943-7900.0000110

Smith, S. J., & Friedrichs, C. T. (2011). Size and settling velocities of cohesive flocs and suspended sediment aggregates in a trailing suction hopper dredge plume. *Continental Shelf Research*, *31*(10, Supplement), S50-S63. https://doi.org/https://doi.org/10.1016/j.csr.2010.04.002

Thorne, P., Vincent, C., Hardcastle, P., Rehman, S., & Pearson, N. (1991). Measuring suspended sediment concentrations using acoustic backscatter devices. *Marine Geology*, *98*(1), 7-16.

Thorne, P. D., & Buckingham, M. J. (2004). Measurements of scattering by suspensions of irregularly shaped sand particles and comparison with a single parameter modified sphere model. *The Journal of the Acoustical Society of America*, *116*(5), 2876-2889. https://doi.org/10.1121/1.1808458

Thorne, P. D., & Hanes, D. M. (2002). A review of acoustic measurement of small-scale sediment processes. *Continental Shelf Research*, *22*(4), 603-632. https://doi.org/https://doi.org/10.1016/S0278-4343(01)00101-7

Thorne, P. D., & Hardcastle, P. J. (1997). Acoustic measurements of suspended sediments in turbulent currents and comparison with in-situ samples. *The Journal of the Acoustical Society of America*, *101*(5), 2603-2614. https://doi.org/10.1121/1.418501

Thorne, P. D., & Meral, R. (2008). Formulations for the scattering properties of suspended sandy sediments for use in the application of acoustics to sediment transport processes. *Continental Shelf Research*, *28*(2), 309-317. https://doi.org/https://doi.org/10.1016/j.csr.2007.08.002

Thorne, P. D., Waters, K. R., & Brudner, T. J. (1995). Acoustic measurements of scattering by objects of irregular shape. *The Journal of the Acoustical Society of America*, *97*(1), 242-251. https://doi.org/10.1121/1.413109

Topping, D., Wright, S., Melis, T., & Rubin, D. (2007). High-resolution measurements of suspended-sediment concentration and grain size in the Colorado River in Grand Canyon using a multi-frequency acoustic system. Proceedings of the 10th International Symposium on River Sedimentation,

Topping, D. J., & Wright, S. A. (2016). *Long-term continuous acoustical suspended-sediment measurements in rivers - Theory, application, bias, and error* [Report](1823). (Professional Paper, Issue. U. S. G. Survey. http://pubs.er.usgs.gov/publication/pp1823

Urick, R. J. (1983). *Principles of Underwater Sound* (3rd ed.). McGraw-Hill. https://books.google.nl/books?id=hfxQAAAAMAAJ

van der Grinten, R. (2019). *Two problems in sediment measurements tackled* Retrieved 23-03-2022 from https://www.nortekgroup.com/news/two-problems-in-sediment-measurements-tackled

Vincent, C. E., Marsh, S. W., Webb, M. P., & Osborne, P. D. (1999). Spatial and temporal structures of suspension and transport over megaripples on the shore face. *Journal of Geophysical Research: Oceans*, *104*(C5), 11215-11224. https://doi.org/https://doi.org/10.1029/1999JC900020

Wang, Z. B., Hoekstra, P., Burchard, H., Ridderinkhof, H., De Swart, H. E., & Stive, M. J. F. (2012). Morphodynamics of the Wadden Sea and its barrier island system. *Ocean & Coastal Management*, *68*, 39-57. https://doi.org/https://doi.org/10.1016/j.ocecoaman.2011.12.022

Wren, D., Barkdoll, B., Kuhnle, R., & Derrow, R. (2000). Field techniques for suspended-sediment measurement. *Journal of Hydraulic Engineering*, *126*(2), 97-104.

Appendix A: Data quality echosounder

Table A. 1 contains measured uncorrected backscatter intensities (R_x; after averaging), noise levels (NT; after averaging) and corresponding signal-to-noise ratios (SNR) for the measurements taken at 1000, 500 and 250 kHz. A threshold of $SNR < 1.1$ was used to discard faulty data, which was most of the 250 data. Therefore, only the measurements taken at 1000 and 500 kHz have been processed further.

#	*Tide*	$R_{x,1000}$ *[dB]*	$R_{x,500}$ *[dB]*	$R_{x,250}$ *[dB]*	NT_{1000} *[dB]*	NT_{500} *[dB]*	NT_{250} *[dB]*	SNR_{1000} *[-]*	SNR_{500} *[-]*	SNR_{250} *[-]*
1	flood	78.30	44.09	15.48	27.17	26.49	15.56	2.9	1.7	1.0
2	flood	93.35	55.60	18.36	24.59	23.45	13.00	3.8	2.4	1.4
3	ebb	61.72	31.75	6.04	20.04	16.63	6.44	3.1	1.9	0.9
4	ebb	65.71	34.75	6.01	20.16	15.49	6.52	3.3	2.2	0.9
5	ebb	78.82	45.57	9.53	25.19	19.24	6.60	3.1	2.4	1.4
6	ebb	84.99	51.59	11.85	22.21	17.20	6.53	3.8	3.0	1.8
7	ebb	63.82	35.42	7.04	19.98	16.69	7.16	3.2	2.1	1.0
8	ebb	66.94	38.53	6.84	20.18	15.98	6.72	3.3	2.4	1.0
9	ebb	73.10	41.32	8.11	20.17	16.12	6.58	3.6	2.6	1.2
10	ebb	72.69	39.82	7.13	20.10	16.19	6.94	3.6	2.5	1.0
11	ebb	64.43	35.92	6.51	20.38	16.62	6.93	3.2	2.2	0.9
12	ebb	69.52	38.62	8.02	20.13	16.85	6.81	3.5	2.3	1.2
13	ebb	75.30	46.24	12.42	20.43	16.95	6.75	3.7	2.7	1.8
14	ebb	63.29	36.51	6.52	20.13	16.51	6.58	3.1	2.2	1.0
15	ebb	63.81	37.18	6.58	20.42	16.49	6.57	3.1	2.3	1.0
16	ebb	66.84	39.49	6.45	20.20	16.73	6.44	3.3	2.4	1.0
17	ebb	81.47	49.54	15.19	19.98	17.61	6.85	4.1	2.8	2.2

Table A. 1: Overview of measured raw backscatter intensities, noise levels and corresponding signal-to-noise ratios for the three frequencies.

Appendix B: Water sample lab analysis

B.1 Lab processing

The water samples were further processed in the lab to determine SSC for the 0.5 L subsamples containing the finer sediment and for the coarser material that remained on the sieve. A detailed description of each step and corresponding measurement uncertainty is given in Table B. 1 for the fine particles and in Table B. 2 for the coarser particles. SSC determined for both classes was then summed to obtain the total values of $M_{s,ref}$, given in Table 6.

B.1.1 Sub-samples containing fine particles

The 0.5 litre subsamples were filtered (paper filters, retention size 0.45 µm) and oven dried at 75 °C for over 48 hours. The filtered content and filter, metal drying tray and plastic storage container were weighed using a precise scale. The mass of the fine sediment fraction was determined by subtracting the empty filter, drying tray and storage container weight which have been determined in advance. Dividing the mass by the subsample volume yielded the fine suspended sediment concentration, SSC_{fine}.

a)

b)

c)

Figure B. 1 Pictures of different steps in the lab process: a) filtration of the 0.5 L subsamples containing the fine suspended material; b) oven drying of the samples and c) weighing of the samples using a precise scale.

Step	Description	Measurement uncertainty (value)	Measurement uncertainty (assumptions)
1a	Determine $M_{tray+filter}$	±0.0003 g	Very short-term (1 minute) fluctuations around ±0.00005 g. Short-term (1 hour) fluctuations around ±0.0001 g. Long-term (weighing on different days, replacing weighed quantity in scale) fluctuations max. ±0.001 g. Representative value of ±0.0003 g.
1b	Determine $M_{container+tray+filter}$	±0.0003 g	See 1a.
2	Separating fine from coarse	-	All fine content (particles with $d < 63$ or 75 μm) retained in filtered water volume
3	Taking 0.5 L subsample	-	Entire sample volume sufficiently stirred before taking subsample
4	Filtration: note precise subsample volume	±5 mL	Volume scale on filtration equipment read with 5 mL uncertainty. All fine content from subsample retained on filter paper.
5	Drying in oven at 75 degrees	-	Trays containing filter and fine content undisturbed during drying process.
6a	Determine $M_{tray+filter+content}$	±0.0003 g	See 1a.
6b	Determine $M_{tray+filter+content}$ Determine $M_{container}$	±0.0003 g ±0.0003 g	See 1a.
7a	$M_{fine} = M_{tray+filter+content} - M_{tray+filter}$		
7b	$M_{fine} = M_{tray+filter+content} - (M_{container+tray+filter} - M_{container})$		
8	$SSC_{fine} = M_{fine}/V_{subsample}$	±1-4 mg/L	

Table B. 1: Overview of steps taken in determining SSC of the fine particle size fraction and the assumptions and introduced measurement uncertainties in each step. The steps highlighted in grey indicate extra steps that have been taken in processing part of the samples.

B.1.1 Coarser material remaining on sieve

Determining the concentration of the coarse material on the sieve was done in two steps. First, the sieved material was oven dried at 75 °C for over 48 hours and weighed. The mass of the material was determined by subtracting the empty drying tray and storage container weight determined before. The concentration of this fraction, SSC_{coarse} was determined by dividing by the total sample volume. For the flood samples, some extra steps were included in the process before determining the weight of the sampled material. This may have had an influence on the measurement uncertainty, which is documented in Table B. 2.

Step	Description	Measurement uncertainty (Δ)	Measurement uncertainty (assumptions)
1	Determine $M_{container+tray}$	±0.0003 g	Very short-term (1 minute) fluctuations around ±0.00005 g. Short-term (1 hour) fluctuations around ±0.0001 g. Long-term (weighing on different days, replacing weighed quantity in scale) fluctuations max. ±0.001. Representative value of ±0.0003 g.
2	Determine V_{sample}	±0.15 L	Reading off bucket volume scale: test measurements (25x) showed a mean difference between estimated volume and real volume (determined by weighing bucket) of 0.09 L, with σ = 0.06 L -> uncertainty = mean + σ
3	Sieving material with $d > 63$ µm or $d > 75$ µm and put in container	-	Uncertainty not quantified, analysed in data processing.
4b	-Determine M_{tray} -Resuspend and sieve content -Drying container + tray + rest material and tray + material in oven at 75 °C for more than 48 hours	±0.0003 g ±0.05 x $M_{sand+other}$ ±0.05 x $M_{sand+other}$	See step 1 Resuspending sample material and sieving adds another 5% uncertainty See step 4a
5a	Determine $M_{container+tray+content}$	±0.0003 g	See step 1
5b	-Determine $M_{container+tray+rest}$ -Determine $M_{tray+content}$	±0.0003 g ±0.0003 g	See step 1
6a	$M_{coarse} = M_{container+tray+content} - M_{container+tray}$	-	Combined uncertainty
6b	$M_{coarse} = M_{tray+content} - M_{tray} + M_{container+tray+rest} - M_{container+tray}$	-	Combined uncertainty
7	$SSC_{coarse} = M_{coarse}/V_{sample}$	±2-12 mg/L	Combined uncertainty
8	Determining M_{coarse}	±0.0003 g ±0.0003 g	See step 1. Determining combined mass PHZD ebb and MG ebb samples before LOI analysis.
13	Total uncertainty SSC_{coarse}	±2-15 mg/L	Combined uncertainty

Table B. 2: Overview of steps taken in determining SSC of the coarse particle size fraction and the assumptions and introduced measurement uncertainties in each step. The steps highlighted in grey indicate extra steps that have been taken in processing of the flood samples.

Appendix C: Sensitivity analysis ΔG

A value of $\Delta G = 31.4$ dB was used for calculation of ΔS_v for all measurements. Table C. 1 presents correlation coefficients for measured vs. predicted S_v' for the MF method applied to the combined ebb and flood measurements for various values of ΔG. For values of $\Delta G < 31.0$ dB, both flood samples were dropped because ΔS_v would be out of the resolvable range. For $31.0 < \Delta G < 31.9$, relatively high correlations were obtained. In hindsight, use of $\Delta G = 31.0$ would have resulted in slightly better results for the 500 kHz data.

ΔG	$r^2_{MF,1000}$	$r^2_{MF,500}$
31.0	0.88	0.74
31.1	0.88	0.72
31.2	0.88	0.70
31.3	0.88	0.69
31.4	0.88	0.68
31.5	0.87	0.67
31.6	0.87	0.66
31.7	0.87	0.65
31.8	0.86	0.64
31.9	0.85	0.63
32.0	0.66	0.50
32.5	0.48	0.39
33.0	0.43	0.36

Table C. 1: Correlations of measured vs. predicted S_v' using the MF model for various values of ΔG (combined ebb + flood measurements).

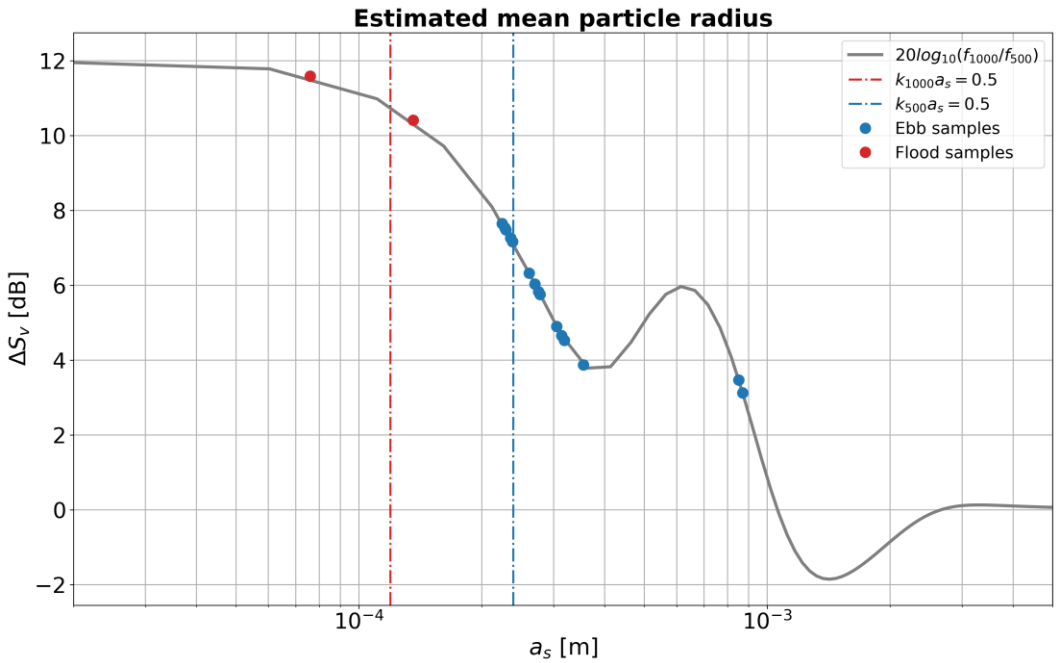

Figure C. 1: Equivalent mean particle radii derived with $\Delta G = 32.5$ dB.

Appendix D: Backscatter and SSC plots

For all combinations of method (SF or MF), measurement set (ebb or ebb and flood) and frequency (1000 and 500 kHz), plots of fitted backscatter relations and corresponding SSC estimations were generated. Figures corresponding to key observations were printed in Chapter 4, other plots are presented here.

D.1 SF 1000 kHz SSC estimations (ebb)

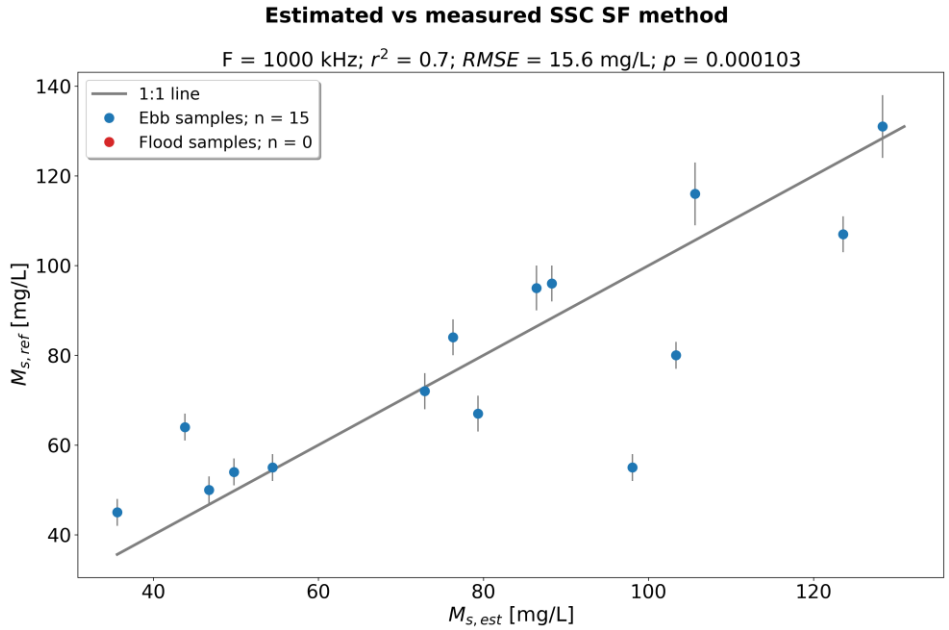

Figure D. 1: SSC estimations based on the SF backscatter relation fitted to the 1000 kHz ebb measurements.

D.2 SF 1000 kHz backscatter relation (combined ebb and flood)

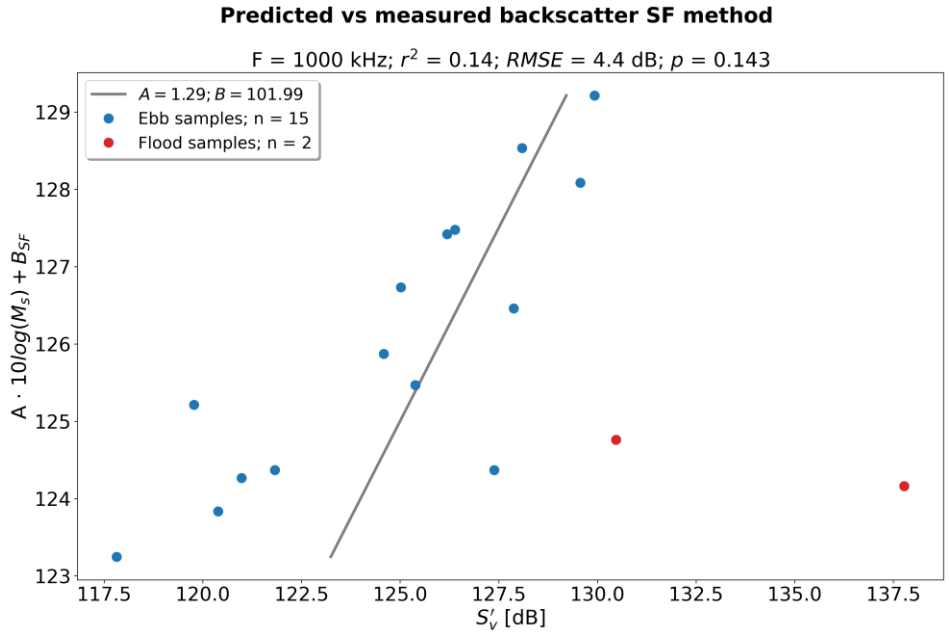

Figure D. 2: SF backscatter relation fitted to the 1000 kHz ebb and flood measurements.

D.3 SF 1000 kHz SSC estimations (combined ebb and flood)

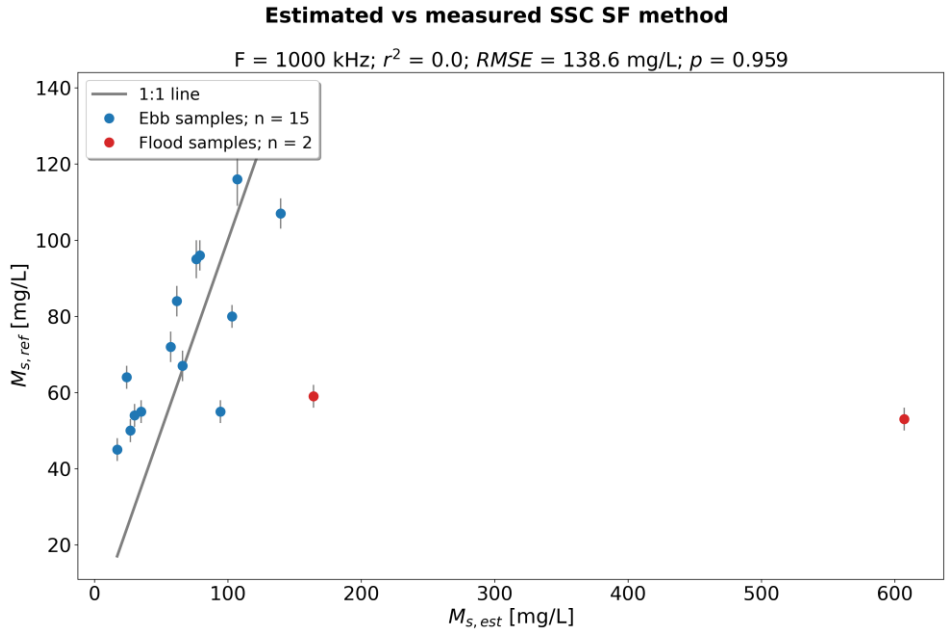

Figure D. 3: SSC estimations based on the SF backscatter relation fitted to the 500 kHz ebb and flood measurements.

D.4 MF 1000 kHz backscatter relation (ebb)

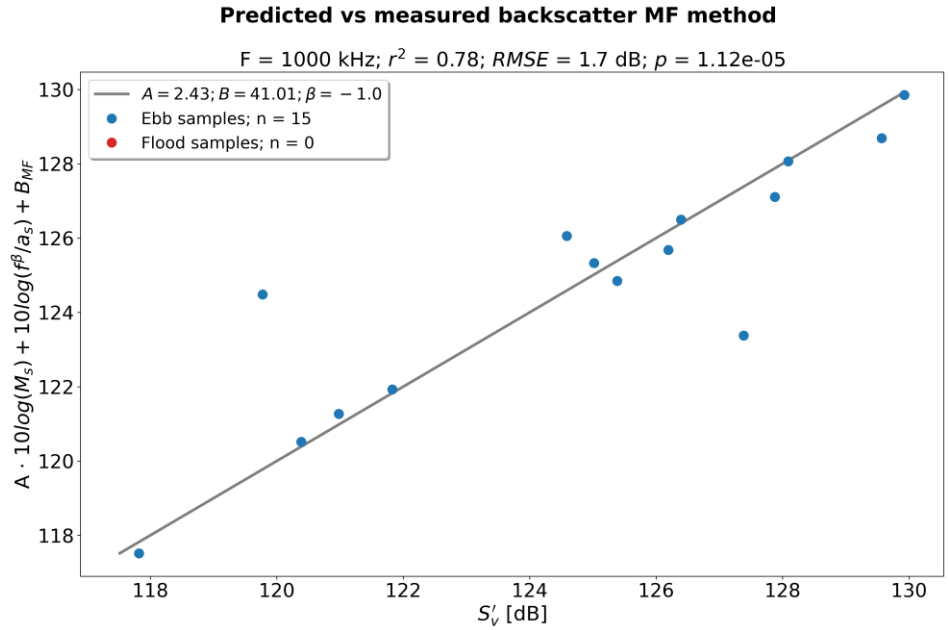

Figure D. 4: MF backscatter relation fitted to the 1000 kHz ebb measurements.

D.5 MF 1000 kHz SSC estimations (ebb)

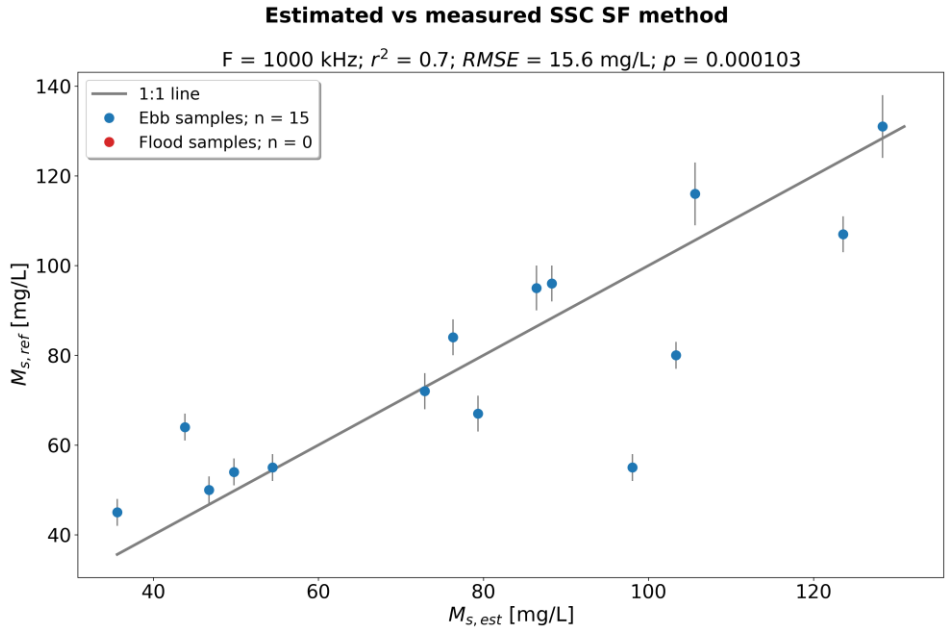

Figure D. 5: SSC estimations based on the MF backscatter relation fitted to the 1000 kHz ebb measurements.

D.6 MF 500 kHz backscatter relation (ebb)

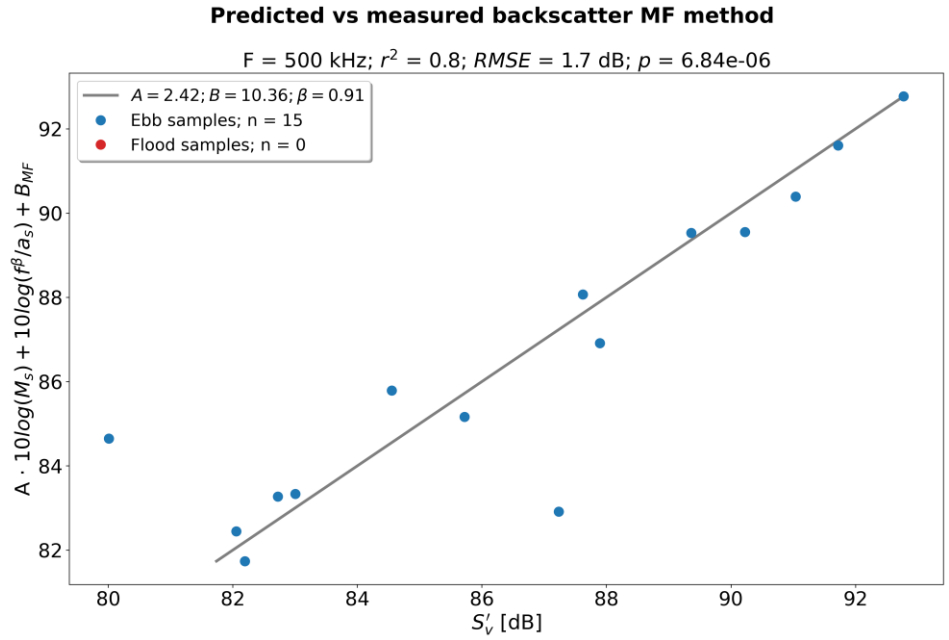

Figure D. 6: MF backscatter relation fitted to the 500 kHz ebb measurements.

D.7 MF 500 kHz SSC estimations (ebb)

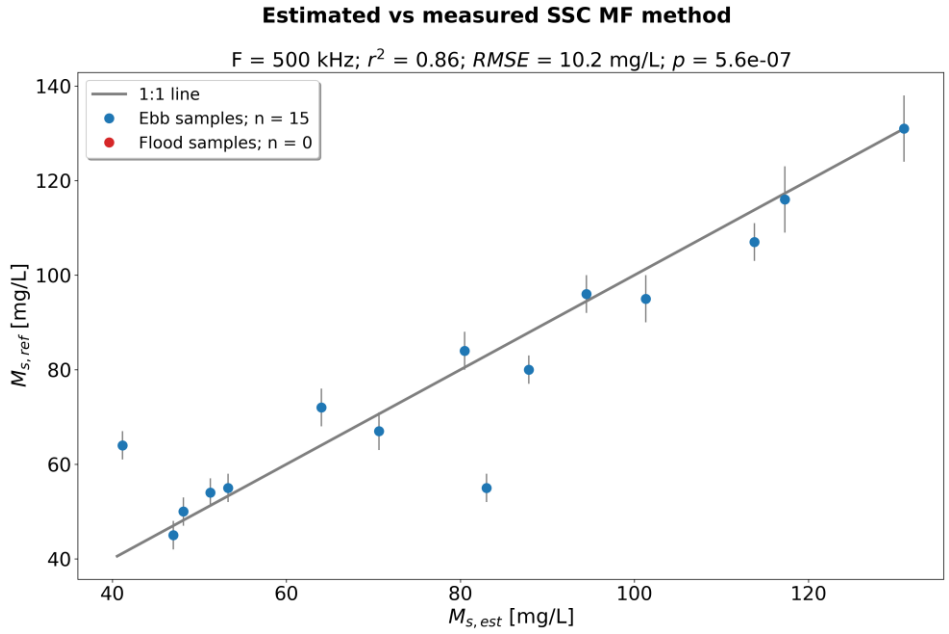

Figure D. 7: SSC estimations based on the MF backscatter relation fitted to the 500 kHz ebb measurements.

D.8 MF 500 kHz backscatter relation (combined ebb and flood)

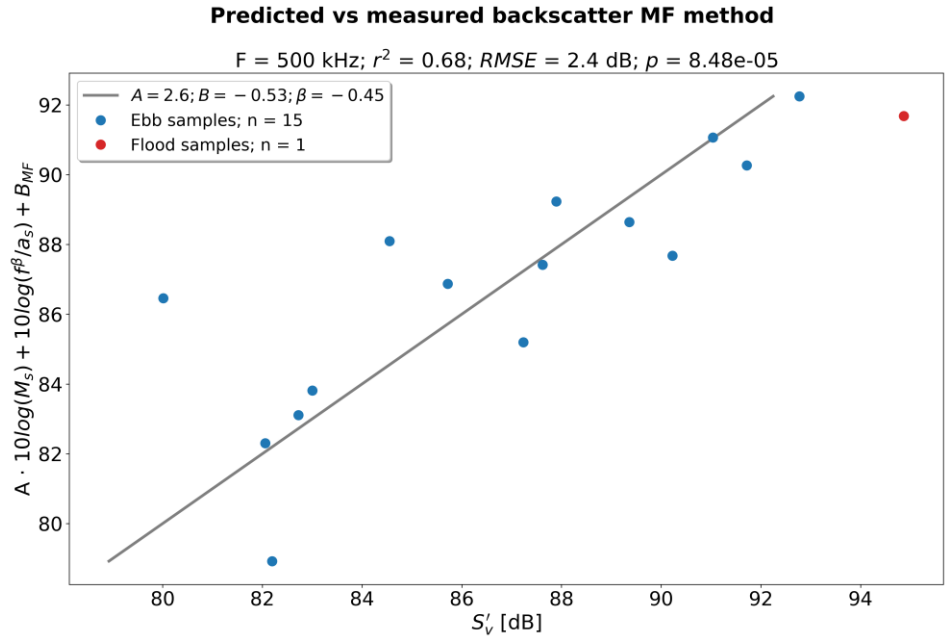

Figure D. 8: MF backscatter relation fitted to the 500 kHz ebb and flood measurements.

D.9 MF 500 kHz SSC estimations (combined ebb and flood)

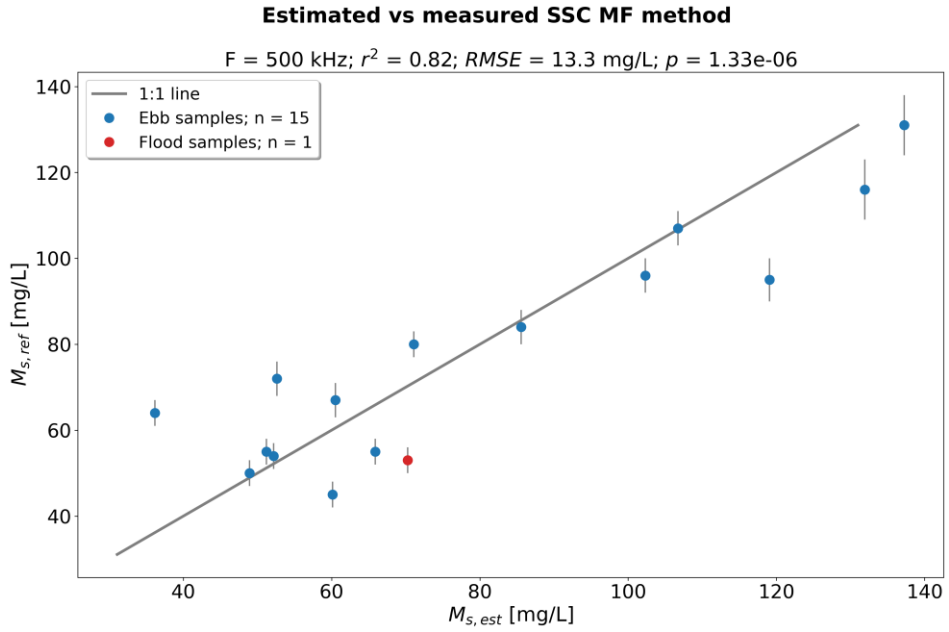

Figure D. 9: SSC estimations based on the MF backscatter relation fitted to the 500 kHz ebb and flood measurements.